AFOSR 66-2726

AD645119

GIANNINI SCIENTIFIC CORPORATION
SANTA ANA DIVISION
3839 SOUTH MAIN STREET, SANTA ANA, CALIFORNIA 92702

GIANNINI SCIENTIFIC CORPORATION

ELECTROTHERMALLY ACCELERATED PLASMA JETS

Final Technical Report FR 096-1572
Covering 1 June 1965 to 31 May 1966
Contract AF 49(638)-1572

For
AIR FORCE OFFICE OF SCIENTIFIC RESEARCH
WASHINGTON, D. C.

Adriano C. Ducati
Principal Investigator

30 September 1966

GIANNINI SCIENTIFIC CORPORATION
Santa Ana Division
3839 South Main Street
Santa Ana, California 92702

ABSTRACT

Experimental and theoretical results are presented on the performance characteristics of the low pressure arc jet operated with hydrogen. Thermal and thrust power efficiency have been measured for up to 20 kilogauss applied magnetic fields and various electrode configurations and specific impulses. The thermal efficiency is insensitive to magnetic field strength and specific impulse in the high range of specific impulse. Thrust efficiency shows a dependence on the magnetic field for operating conditions which produce values of the Hall parameter much larger than unity, but this may be due to the much discussed spurious interactions of the arc with the environment.

The efficiencies show a definite and fairly regular increase with increasing arc chamber pressure. Tests have been conducted which demonstrate qualitatively the effect of the applied field on the arc current distribution.

A good two-parameter fit of thermal efficiency data is given, and an analytical model for the thermal losses is partially developed. Explicit expressions for the torque on the arc jet flow are obtained for two classes of idealized current distributions. An inequality is derived which places a lower bound on the torque for a given applied magnetic field and electrode configuration.

TABLE OF CONTENTS

ILLUSTRATIONS

ILLUSTRATIONS (cont.)

ILLUSTRATIONS (cont.)

ILLUSTRATIONS (cont.)

TABLES

1.0 DEVELOPMENT OF THE WORK

1.1 Time Schedule of Contract AF 49(638)-1572

This contract was started on 1 June 1966 for a period of 12 months. The work was terminated on 31 May 1966.

1.2 Status at the Beginning of the Work

The work presented in this report is a continuation of a preceding investigation.[1] The state of progress at the termination of this prior work, for convenience, is summarized here.

Low temperature jets were produced by employing a resistive heating method. The acceleration of the propellants H_2, He, NH_3, N_2, O_2 and A was studied and specific impulse measurements were obtained over a 300 to 2800°K temperature range. Various thrustor configurations, produced by changing throat lengths, throat diameters and nozzle configurations were tested. A large number of tests were conducted using a short orifice without a supersonic nozzle. In this case the thermal and viscous losses are small and if the flow is nonreacting, the theory is very simple and permits a comparison of theory and measurements. Good agreement between the measured and predicted values was obtained. During the course of the low temperature studies, methods were developed for measuring the stagnation temperature near the high temperature limit of operation with resistive heaters.

High temperature plasma jets were obtained by using the arc heating method. Tests, almost exclusively with hydrogen propellant, were conducted over a 3000 to 10,000 second specific impulse range. Characteristic properties of this type of arc jet are that it operates very well at low mass flow rates, low chamber pressures and high currents (as much as 3000 amps). At these low gas pressures and high currents the magnetic and gas kinetic pressure forces are comparable and magnetic effects are expected to be

important. Indeed, the effects of self-pinching of the plasma were observed near the cathode. It has been found that in the low pressure high current regime the cathode current distribution becomes very diffuse, a condition which is undoubtedly crucial for the passage of such large currents through the cathode. The magnetic forces can be essential for determining the structure of the arc and, moreover, may be significant in the transfer of electrical to kinetic and thermal plasma energy.

The major part of the high temperature testing was conducted at a 25 mg/sec mass flow rate. In these tests the thermal efficiencies were found to be between 60 and 70 percent. The thrust efficiencies were less than the frozen flow efficiency and, with increasing specific impulse, followed roughly the increase of the frozen flow efficiency.

An investigation on the effects on the arc jet performance of a moderate strength magnetic field applied coaxially to the electrode geometry was initiated. The applied field, by confining and guiding the flow along magnetic field lines, appears to act very much like a nozzle. The Lorentz force produced by the interaction of the arc currents with the applied magnetic field causes the plasma to rotate. A more uniform current distribution, which is apparently due to this rotation, results. The arc voltage was found to increase linearly with the magnetic field strength up to values of 2000 gauss, an arc characteristic which has been observed in other laboratories (see e.g., (2) and (3)). The linear increase in voltage was faster the larger the throat diameter.

These initial tests did not indicate a strong dependence of efficiency on magnetic field strength; however, the data were too few to form firm

conclusions. Part of the continued program was devoted to repeating and extending the efficiency measurements over a much larger range of arc parameters and magnetic field strengths.

Operating at high currents introduced the possibility of electromagnetic interactions occurring which could introduce errors in the thrust measurements. Steps were taken to eliminate this possibility with the development of a device called the "thrust killer." It collects and cools the jet and directs the flow normal to the thrust direction. This eliminates the thrust accurately enough so that unwanted electromagnetic forces can be detected and eliminated under actual operating conditions.

During this program additional problems peculiar to the low pressure, high current operation were encountered, namely, the ingestion and acceleration of ambient gas and the vaporization and acceleration of electrode material. A spectroscopic analysis of the jet plume was conducted which showed that both ambient gas and electrode material were present in the plume in significant quantities at conditions of very low mass flow rate. Furthermore, the analysis showed that the region of energy addition extended well outside the thrustor exit plane.

Recommendations for future work emphasized the study of the region of the arc external to the thrustor. The problem of heat transfer to the anode was suggested as an important area for further experimental and theoretical work. The need for a more complete investigation of the effects of an applied magnetic field on arc jet performance was pointed out.

1.3 Basic Results

The work discussed here is a continuation of the investigation of the low pressure, high current arcs summarized in Section 1.2. The measurements reported here are the initial results of a larger, planned program which extends over twenty different geometries, four specific impulse levels, six magnetic field intensities and five different mass flow rates. The completion of the planned program will require a long testing period. The results given here are for a single mass flow rate (10 mg/sec) with several electrode geometries at various specific impulses and magnetic field strengths.

Significant results which have been obtained are the performance measurements over a 1 to 20 kilogauss range of applied magnetic field strengths. These results extend the experimental knowledge of the effect of the applied field much beyond the range previously reported.[1-6] It had been hoped that the magnetic field, applied coaxially to the thrustor, would reduce the thermal losses. These measurements show that this is not the case; the thermal efficiency was found to be approximately independent of the field (and specific impulse) in the high range of I_{sp} (4000 sec). The thrust efficiency shows a tendency to increase with magnetic field at constant I_{sp}, but definite conclusions are not possible at this time because of the much discussed problem[1, 2, 4, 5] of the arc interaction with the environment. Even with these uncertainties it appears that the thrust efficiency is limited by the frozen flow efficiency, and that the magnetic field acts as a nozzle while imparting angular momentum to the flow.

Part of the work was devoted to the study of conditions which can produce anomalies in the arc jet performance. It is now reasonably certain that increasing the magnetic field causes the currents to be distributed more and more outside the electrode zone. This condition probably favors the occurrence of unwanted interactions. Our ideas about the current distribution and anomalies are inferred mainly from visual and photographic observations; more quantitative measurements, such as a direct measurement of the current distribution, have not been attempted. A method which records simultaneously a photograph of the arc and the values of the principal arc variables (power, voltage, etc) has aided in correlating the appearance of the arc with performance measurements. Under certain conditions, observations show that discharges to the test tank can develop. Glow discharges and arcing have been observed. Obviously, care must be taken to insure that these secondary effects do not produce misleading performance results. The installation, proposed here some time ago, of a large insulated tank would eliminate interactions of this kind. Toward this end, the design and construction of facilities using existing tanks containing an insulating section has been initiated. The construction of a special nonmagnetic tank with an interior heavily coated with plastic material has also been initiated. The effect of the insulation will be studied in a continued program. In addition, both electrode vaporization and gas entrainment can contribute to anomalies. If electrode vaporization takes place, one can weigh the electrodes before and after a test to correct for this contribution to the flow. However, a reliable quantitative method to determine the effects of entrainment does not exist presently.

The effect of the applied magnetic field on the flow has also been studied analytically. It is known that the momentum equation for a highly conducting gas in a strong, axial field, shows that the Lorentz forces should just balance the centrifugal and pressure forces on the plasma, thus confining and guiding the flow in much the same way as a metal nozzle. It is also known (see e.g., (5)) that the interaction of the applied field with "radial" currents produces an azimuthal force and subsequent rotational motion of the plasma.

The rotational motion of the plasma has been considered further here. We have found solutions of the angular momentum equation for two classes of idealized current distributions. These solutions give the total torque on the flow in terms of the arc current and the flux through certain definite regions of the flow. An inequality has also been derived which places a lower limit on the angular momentum imparted to the flow for a given arc current and magnetic field. This inequality holds under quite general conditions. The inequality is derived from the assumptions of an axisymmetric, steady state, inviscid, scalar pressure, electrically neutral, plasma flow. The transfer of electrical power to rotational motion is of particular interest because this energy transfer need not proceed by the ohmic heating process, but can go from the electric field to the ions without the intermediary of collisions.

The thermal efficiency problem has also been studied. A correlation of the thermal efficiency measurements has been obtained by assuming that the electrode power loss is equal to the sum of a constant radiation term

plus a term proportional to the stagnation power of the flow. This form of the power loss permits a two-parameter fit of the data; a good fit is obtained over the entire range of thermal measurements made here and also of some measurements performed at another laboratory.[2]

An analytical model for the heat loss is considered which applies for conditions of strong applied field and a highly ionized plasma. The anode losses are seen to arise from electron transport along the magnetic field lines in the peripheral region of the flow. According to this model, the anode loss is associated with a ratio of anode voltage to total voltage which is independent of power and also independent of applied magnetic field strength.

The dependence of thrust efficiency on mass flow is discussed and its relevance to the entrainment problem is considered. A different aspect of the problem of the control of entrainment is pointed out.

2.0 EXPERIMENTAL WORK

2.1 Improvement of Testing Facilities

The vacuum system used in the preceding period is described in Reference 1 where the suggestion for the construction of a new huge system, made basically with insulating materials, can also be found. For economic reasons it has been impossible to follow these suggestions and only minor modifications have been adopted. The pumping system, with a total capacity of 4500 liters/sec, has remained unchanged with the exception of a complete leak control of all the connections and the shortening and increase in diameter of the pipes to the testing chamber. Because of the great number of tests anticipated, special care has been taken to design a system capable of fast interchange of plasma heads. Water-cooled coils and relative connections capable of a load of over 5000 amps without interfering with the thrust measurements have been constructed which produce magnetic fields of over 20 kilogauss. Ample water-cooling of all the arc connections and suspensions has been installed to avoid any shift of the zero reading up to an input power of 200 kw. A magnetic dampener of large dimensions has been applied to the thrust stand to increase the precision of the readings and to reduce the measurement time. A special photographic setup has been constructed which is capable of recording simultaneously the actual picture of the arc plume and six basic instruments (current, voltage, thrust, arc pressure, chamber pressure and flow). The accuracy of any single measurement has been improved and tested for reproducibility in various conditions.

Figures 1 to 4 show schematically the various modifications introduced in the vacuum facility used during the tests reported here. The experimental chamber is not insulated and uses only partially nonmagnetic materials. Toward the end of the period it was considered useful to enclose in the main vacuum tank a secondary tank made with insulating materials, as illustrated schematically in Figure 5. Initially, this insulated chamber was made with asbestos based materials which contained a large amount of impurities. The long degassing period required before the regular vacuum level could be attached permitted only a reduced number of tests before the end of this work, so its true behavior will be determined during the next period. A test chamber and thrust stand made exclusively of nonmagnetic materials and insulated with a good dielectric layer (as illustrated in Figure 6) has also been initiated during the period and will become the main testing facility during the next work. Refinements of the thrust stand which permit the detection of zero shifts in any direction have been introduced with very stable and reproducible indications as illustrated in Figure 7. This simple mechanical control improves the function of the differential transformer used for the thrust measurements and has proved very useful for constant operation from the same zero position. Another improvement applied to the thrust stand has been the possibility to rigidly block the thrust stand without modifying its zero position. This is particularly useful during the manipulation of the thrustor in changing electrodes and so forth. The blocking arrangement is illustrated in Figure 8.

Because of the great variety of electrode geometries used in the tests (twenty anodes and twenty cathodes as illustrated in Figures 9 and 10),

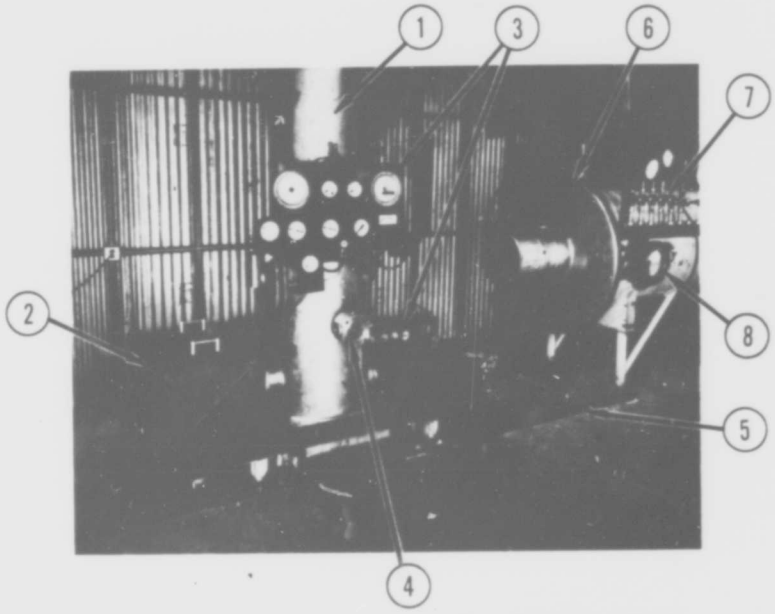

1. Thrust Stand
2. Magnetic Dampener
3. Instrument Panels
4. Thrust Sensing Mechanism
5. Guiding Rail
6. Vacuum Exhaust Tank
7. Cooling Water Manifold
8. Camera Viewing Window

Figure 1. Photograph of Modified Vacuum Facility Used During Testing

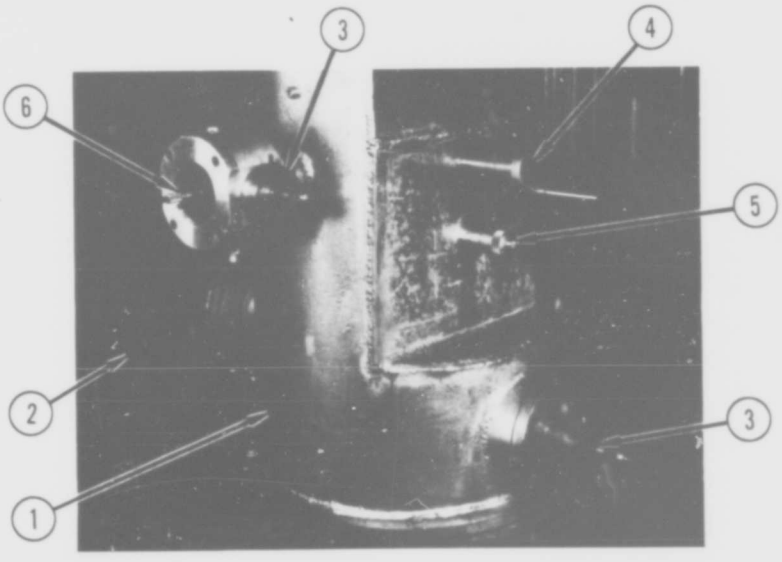

1. Thrust Stand
2. Magnetic Dampener (housing)
3. Thrust Sensing Mechanism
4. Thrust Balance Blocking Mechanism
5. Mechanical Zero Positioner (axial)
6. Mechanical Zero Positioner (horizontal)

Figure 2. Close-up Photograph of Thrust Stand Showing Attached Modifications

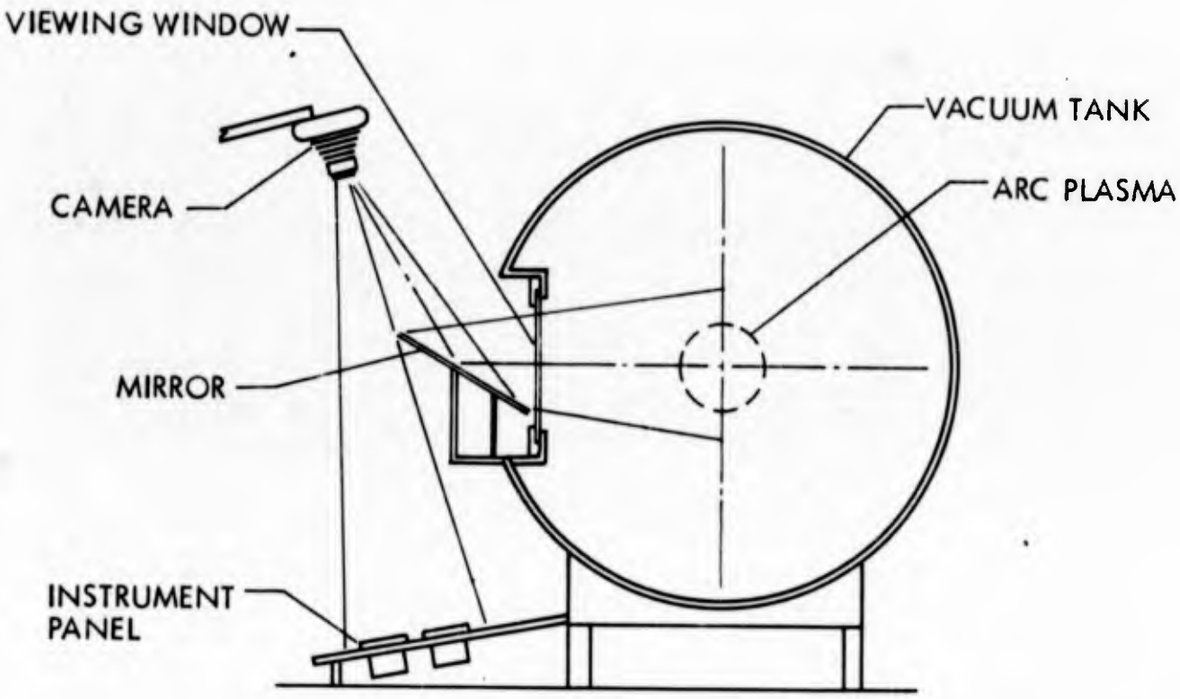

Figure 4. Schematic of Test Setup for Simultaneous Photographic Recording of Plasma Exhaust and Instrumentation

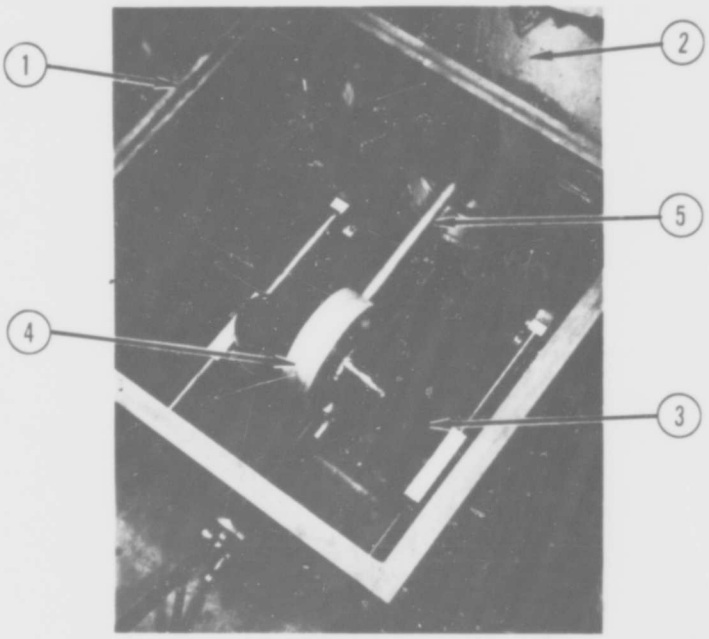

1. Steel Housing
2. Thrust Stand
3. Permanent Magnet
4. Suspended Aluminum Breaking Disc
5. Supporting Rod (attached to thrust balance)

Figure 3. Photograph of Magnetic Dampening Mechanism Attached to Thrust Stand

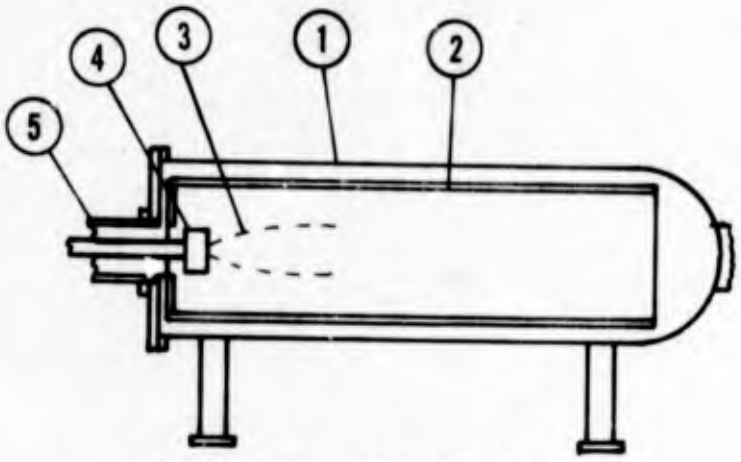

1. Vacuum Exhaust Tank
2. Insulation Lining
3. Arc Plasma
4. Thrustor
5. Thrust Stand Connection

Figure 5. Schematic of Vacuum Tank Showing Enclosed Insulation Lining

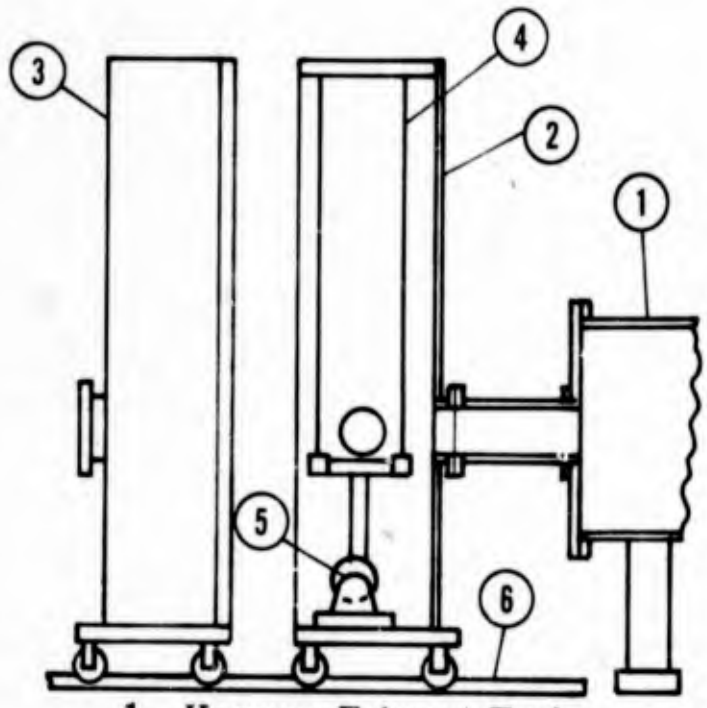

1. Vacuum Exhaust Tank
2. Thrust Stand
3. Removable Enclosure
4. Thrust Balance
5. Magnetic Dampener
6. Guiding Rails

Figure 6. Schematic of New Vacuum Test Facility Constructed Entirely of Nonmagnetic Material

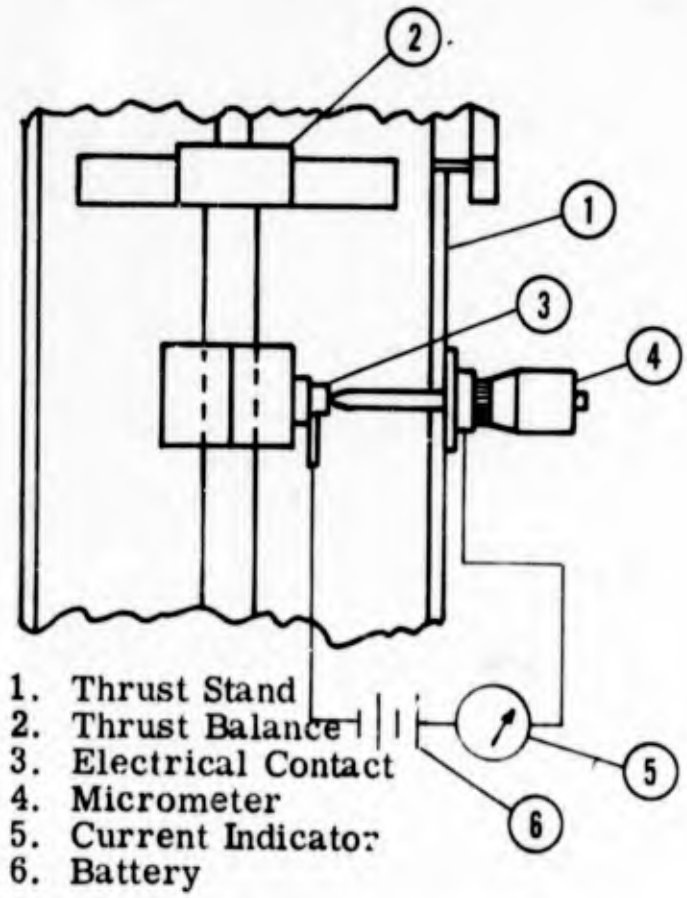

1. Thrust Stand
2. Thrust Balance
3. Electrical Contact
4. Micrometer
5. Current Indicator
6. Battery

Figure 7. Schematic of Axial Zero Shift Indicator Attached to Thrust Stand

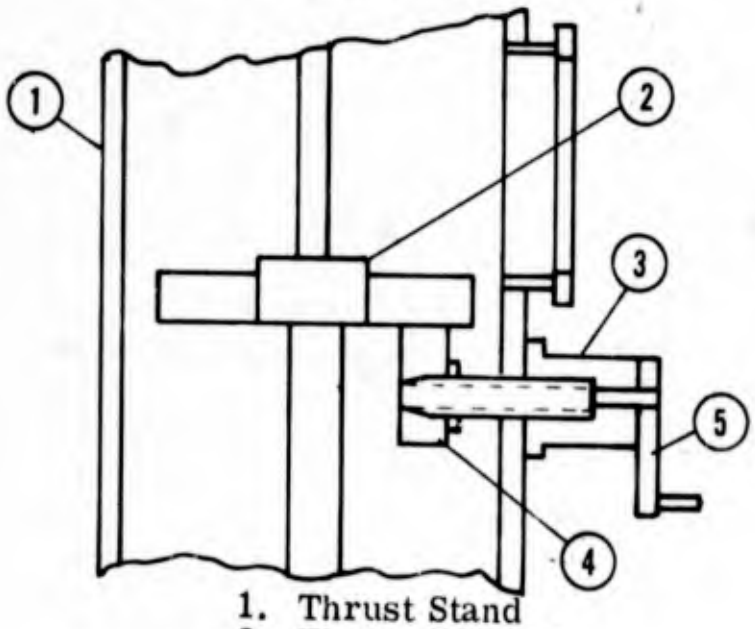

1. Thrust Stand
2. Thrust Balance
3. Bearing
4. Lock Nut
5. Lock Screw

Figure 8. Schematic of Thrust Balance Blocking Device Attached to Thrust Stand

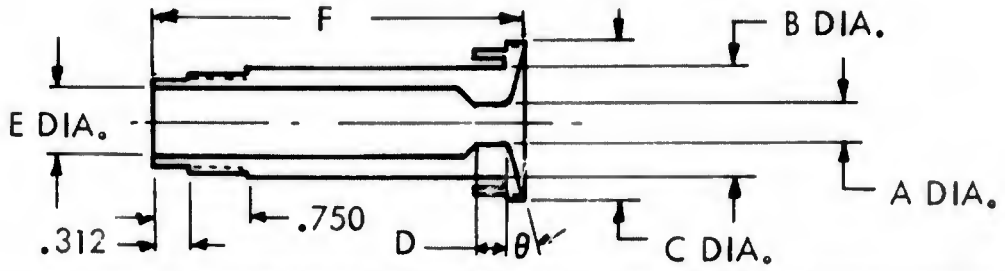

NO.	A DIA	B DIA	C DIA	D	E DIA	F	θ°
1	0.125	1.375	2.500	0.125	0.562	4.125	32
2	0.125	1.375	2.500	0.187	0.562	4.125	32
3	0.125	1.375	2.500	0.250	0.562	4.125	32
4	0.125	1.375	2.500	0.500	0.562	4.125	32
5	0.250	1.375	2.500	0.250	0.625	4.125	33
6	0.250	1.375	2.500	0.375	0.625	4.125	33
7	0.250	1.375	2.500	0.500	0.625	4.125	33
8	0.250	1.375	2.500	1.000	0.625	4.125	33
9	0.500	1.375	2.500	0.500	0.950	4.125	32
10	0.500	1.375	2.500	0.750	0.950	4.125	32
11	0.500	1.375	2.500	1.000	0.950	4.125	32
12	0.500	1.375	2.500	2.000	0.950	4.125	32
13	1.000	1.375	2.500	1.000	1.062	4.125	35
14	1.000	1.375	2.500	1.500	1.062	4.125	35
15	1.000	1.375	2.500	2.000	1.062	4.125	35
16	1.000	1.375	2.500	4.000	1.062	6.250	35
17	2.000	2.375	3.500	2.000	1.062	4.125	0
18	2.000	2.375	3.500	3.000	1.062	5.250	0
19	2.000	2.375	3.500	4.000	1.062	6.250	0
20	2.000	2.375	3.500	8.000	1.062	10.250	0

Figure 9. Dimensions of Interchangeable Anodes to be Used During the Overall Experimental Program

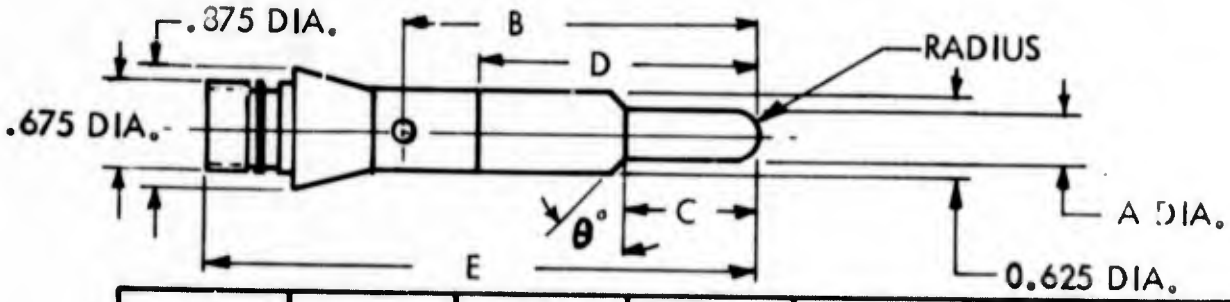

NO.	A DIA	B	C	D	E	RADIUS	θ°
1	0.250	4.750	2.375	4.250	6.375	0.125	45
2	0.250	4.750	2.312	4.250	6.312	0.125	45
3	0.250	4.750	2.250	4.250	6.250	0.125	45
4	0.250	4.750	2.000	4.250	6.000	0.125	45
5	0.500	4.750	2.250	4.250	6.250	0.250	45
6	0.500	4.750	1.875	4.250	5.875	0.250	45
7	0.500	4.250	1.750	3.750	5.750	0.250	45
8	0.500	4.250	1.250	3.750	5.250	0.250	45
9	0.500	4.750	2.250	4.250	6.000	0.250	30
10	0.500	4.000	1.500	3.500	5.250	0.250	30
11	0.500	3.750	1.250	3.250	5.000	0.250	30
12	0.500	2.750	0.250	2.250	4.000	0.250	30
13	0.625	5.000	4.750	4.750	6.000	0.312	0
14	0.625	3.500	3.250	3.250	4.500	0.312	0
15	0.625	3.000	2.750	2.750	4.000	0.312	0
16	0.625	1.000	0.750	0.750	2.000	0.312	0
17	0.625	2.250	2.000	2.000	10.000	0.312	0
18	0.625	2.250	2.000	2.000	7.000	0.312	0
19	0.625	2.250	2.000	2.000	6.000	0.312	0
20	0.625	1.250	1.000	1.000	2.000	0.312	0

Figure 10. Dimensions of Interchangeable Cathodes to be Used During the Overall Experimental Program

fast interchangeability has been studied, together with simplicity of construction. In all the tests conducted in the past the greatest part of the operating time was consumed in the change of the electrodes, while with the new improvement this operation requires only a fraction of the time. Figures 11 and 12 show the detail of anode and cathode with fast interchangeability. The magnetic coil used during this period requires about 150 kw at the maximum value of field strength. Entering the cooling water along one connection and discharging it through the other, the thermal symmetry was impaired (inlet cold and outlet very hot). For this reason the symmetrical solution of Figure 13 was adopted with good results. Subdivision of the cooling in various sections of the coil produced still better performance.

Another important measurement which requires improvement is the measurement of the arc chamber pressure. If a regular pressure gauge is used, the connection must be made directly to the arc chamber with a pipe of relatively large diameter to be able to follow rapid changes of the pressure. A better solution would be to fix a pressure gauge or a transducer directly to the arc chamber (Figure 14). During the first part of the tests difficulties based on these details produced a series of arc chamber pressure data that are not reliable. As will be described later, during the tests, especially when the current paths were outside of the electrodes, glow discharges and sometimes arc discharges appeared in the metallic parts of the thrust suspension. A complete insulation of all these parts has been necessary to reduce the intensity of this effect (Figure 15). A better solution has been developed with the use of a very flexible insulating membrane between the vacuum test chamber and the thrust stand as illustrated in Figure 16.

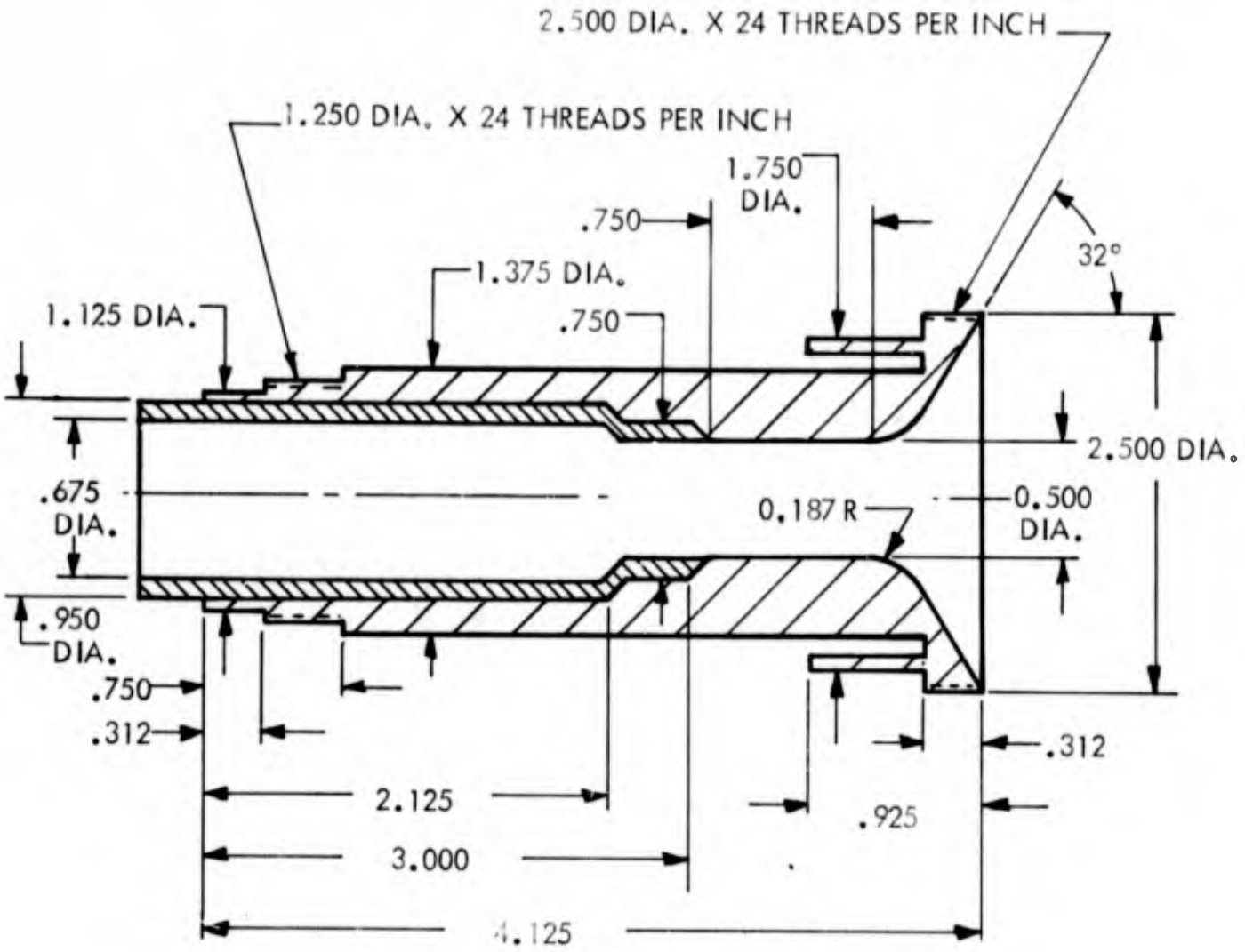

Figure 11. Detailed Drawing of Interchangeable Anode

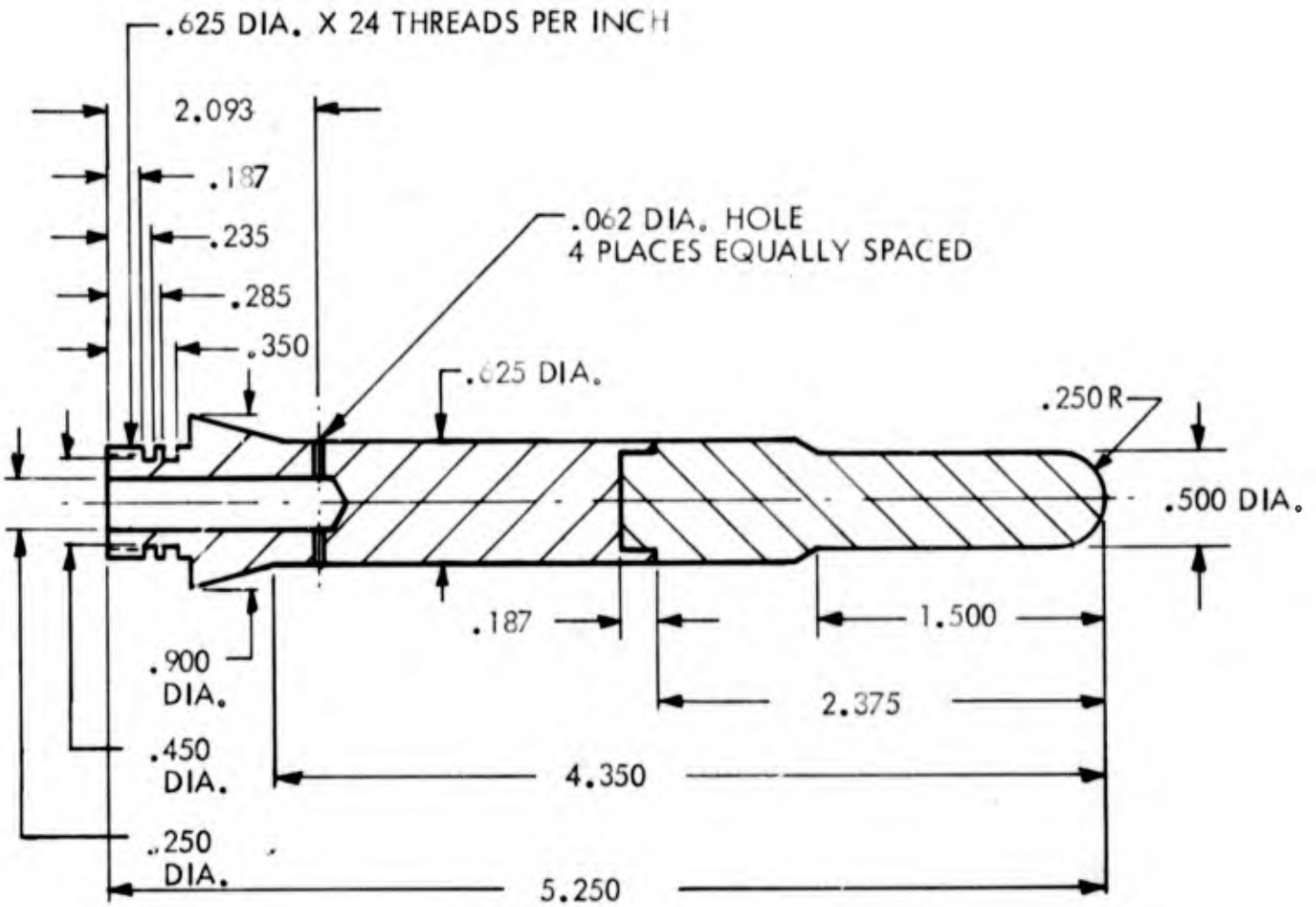

Figure 12. Detailed Drawing of Interchangeable Cathode

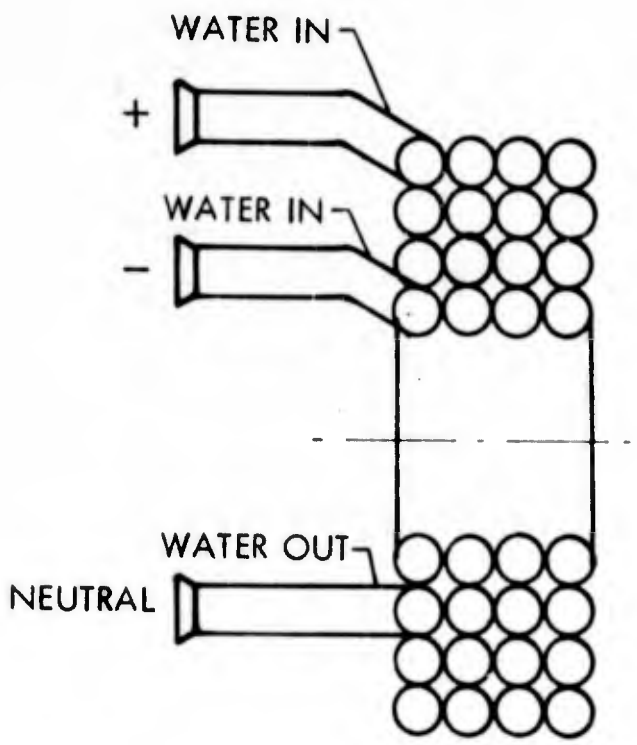

Figure 13. Schematic of External Magnetic Field Coil Showing Series Power Connection With Center Tap Cooling Water Outlet

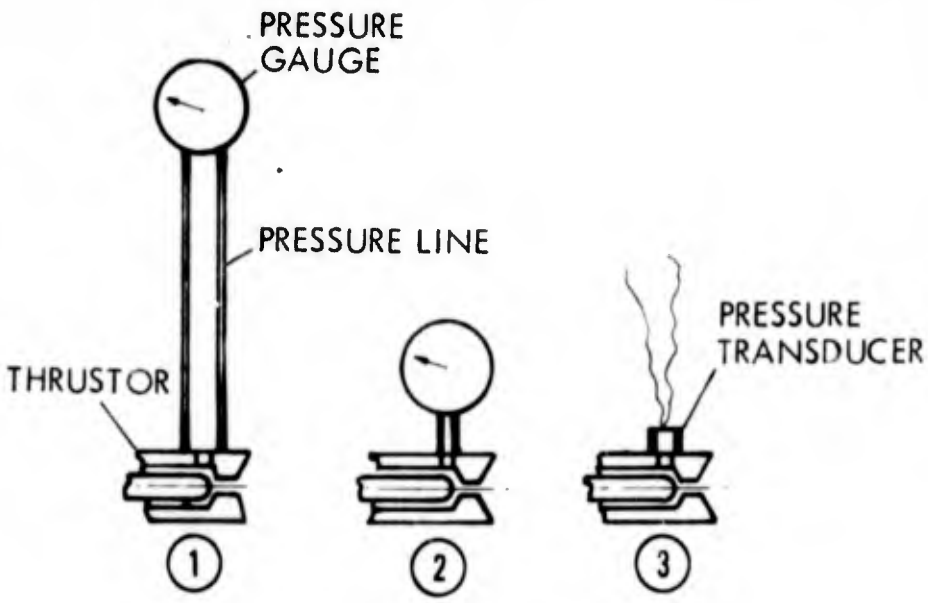

1. Remote Pressure Reading (long wide connection)
2. Local Pressure Reading (narrow short connection)
3. Remote Pressure Reading (transducer locally applied)

Figure 14. Schematic of Applied Methods for Fast Response Measurement of Low Range Arc Chamber Pressure

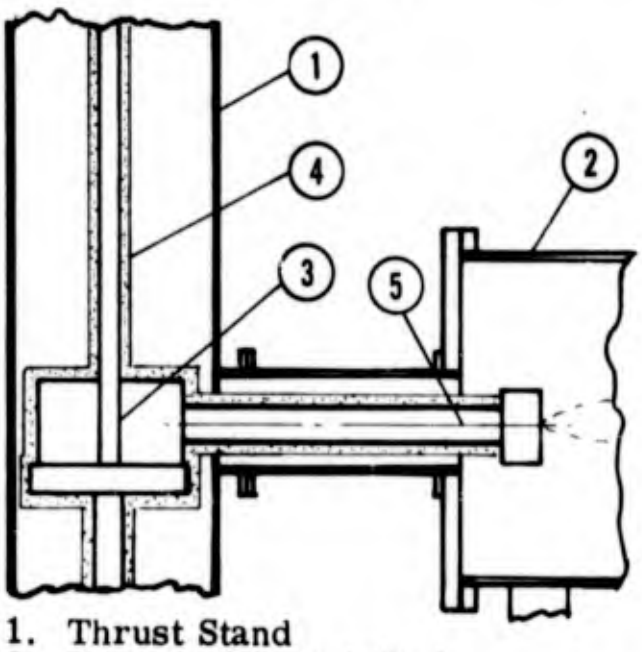

1. Thrust Stand
2. Vacuum Exhaust Tank
3. Thrust Balance and Feed Lines
4. Insulation
5. Thrustor

Figure 15. Schematic of Thrustor Suspension System With Applied Insulation Coating to Prevent Glow Discharge

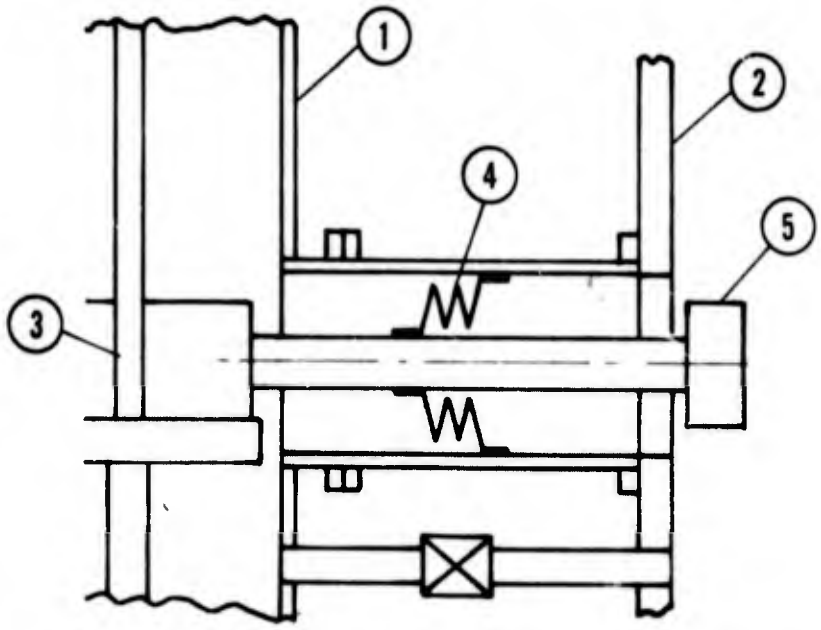

1. Thrust Stand
2. Vacuum Exhaust Tank
3. Thrust Balance and Feed Lines
4. Insulating Membrane
5. Thrustor

Figure 16. Schematic of Thrustor Suspension System in Vacuum Tank With Attached Insulating Membrane

2.2 Conduction of the Tests

The planned program includes the testing of twenty electrode geometries at four specific impulse levels with six magnetic field intensities and five different mass flow rates. This constitutes a monumental group of about 2500 tests for each propellant to be studied. For control purposes, at least two tests are necessary for each point and this brings the total of tests to about 5000. With the old system the change from one experiment to the next implied various hours of preparation. This would bring the total testing time to many years. For this reason the fast interchange system has been devised which reduces the interval between tests to a fraction of the preceding one. This will permit the completion of the program in a much shorter time. Effectively, the total number of usable testing points is smaller than the estimated one because for some fringe points a stable and reliable test cannot be run without disturbing the final results. But for these fringe points the test must be done anyway and eventually repeated before discarding it, so the total number remains as estimated.

When the time to pass from one testing condition to the next was very long, it seemed to be convenient to conduct all possible tests for each set of electrodes assembled before disassembling them. Practically, this solution proved to be poor because a continuous variation of parameters such as mass flow, power, etc., during each test was difficult and unreliable, and precise control of the variation of the geometrical dimensions between tests was not attained, whereby errors could be introduced in the final results. For this reason it has been decided to do each test while separately

controlling any parameter before and after any test and to permit this, the fast interchange system is a basic condition. Considering that tests at constant mass flow are easier to conduct in immediately succeeding runs, it has been decided to run all the tests for one mass flow at a time. Successively all the tests are to be repeated for all the different mass flows involved. In particular, during this contract period a hydrogen mass flow of 10 mg/sec has been used. It appeared at the beginning that as soon as it was decided what the mass flow to start with is (in our case 10 mg/sec), the best procedure is to test successively all the twenty geometries. While this procedure seems to be preferred, as soon as one complete set of data is available during the initial period (10 mg/sec mas flow runs) it has been considered useful to skip some geometrical dimensions to have some general orientative data in a shorter time. For this reason only four diameters of the designed five have been tested and only one length of the designed four has been used during the initial tests. A ratio length/diameter of 1.5 has been chosen, this being one of the most common used in practice.

The program of the test during this first period has been to start from the minimum specific impulse (always at a mass flow of 10 mg/sec) and cover successively all the geometries available and then record for each one of them all the experimental values for each parameter that can influence the interpretation of the results. The principal parameters directly recorded to date are pressure, voltage, current, power input, power in gas and thrust. Others are computed from them. Because of the great number of data a condensed table has been designed capable of containing a great amount of data in a minimum of space. Table 1 is an example of the

table to be used when the test of all twenty geometries is completed. For each specific impulse and mass flow a similar table will be prepared. Specifically, the tables obtained for the four different geometries tested are illustrated in Tables 2 through 6, while Tables 7 and 8 show the calculated thermal and thrust efficiencies. Table 9 is a complete table of the data obtained to date operating at a mass flow of 10 mg/sec with hydrogen, for four specific impulses and four different geometries. The data in Table 9 has been obtained in a noninsulated vacuum tank made only partially of nonmagnetic materials. A second identical series of tests will be made at the beginning of the next period using an insulated secondary vacuum chamber contained in the main metal chamber and both results will be compared. It is hoped that by using the relatively high length to diameter geometrical ratios, the influence of the metal tank will be minimized.

The test procedure now is as follows: After installation of the electrode geometry to be tested the lower specific impulse conditions are reached at the selected mass flow. Readings at six different specified magnetic fields for all the desired parameter values are taken. The readings are repeated three times for reliability of the recorded data, then the operation is interrupted for a short period to check the zero readings and recalibrate the thrust balance. The second specific impulse value is then reached and the series of measurements repeated until a new calibrating interval is reached.

Marginal working conditions are left for the last part of the experiments to reduce the danger of a premature failure of the electrodes under test.

TABLE 1

DATA TABLE FOR PLANNED TESTS WITH TWENTY GEOMETRIES

I_{SP} - 1000 H_2 MASS FLOW - 10 MG/SEC							
Throat		ARC PRESSURE MM kilogauss					
Diam.	Length	1	2	4	8	16	20
0.125	0.125						
0.125	0.187	156	154	152	150	142	+
0.125	0.250						
0.125	0.500						
0.250	0.250						
0.250	0.375	36.0	37.0	31.0	28.0	+	+
0.250	0.500						
0.250	1.000						
0.500	0.500						
0.500	0.750	26.0	24.6	23.5	21.5	18.9	19.0
0.500	1.000						
0.500	2.000						
1.000	1.000						
1.000	1.500	7.3	7.0	6.6	7.0	7.0	6.5
1.000	2.000						
1.000	4.000						
2.000	2.000						
2.000	3.000						
2.000	4.000						
2.000	8.000						

TABLE 2

CHAMBER PRESSURE MEASUREMENTS

Throat Inches	ARC PRESSURE MM kilogauss					
	1	2	4	8	16	20
Isp, sec 1000						
0.125	156	154	152	150	142	+
0.25	36.0	37.0	31.0	28.0	+	+
0.5	26.0	24.6	23.5	21.5	18.9	19.0
1.0	7.3	7.0	6.6	7.0	7.0	6.5
2.0						
Isp, sec 2000						
0.125	-	-	190	198	194	190
0.25	48.0	52.0	40.0	38.0	+	+
0.5	27.0	26.0	25.0	23.0	24.0	20.5
1.0	6.5	6.0	4.0	4.5	5.5	-
2.0						
Isp, sec 4000						
0.125						
0.25	-	-	50.0	48.0	+	+
0.5	-	31.0	28.0	25.8	25.6	26.0
1.0	7.5	7.5	4.8	4.5	-	-
Isp, sec 8000						
0.125						
0.25						
0.5	-	-	29.0	29.5	28.5	27.5
1.0	-	6.7	7.5	7.5	-	-
2.0						

L/D = 1.5

TABLE 3

MEASURED VOLTAGE CHARACTERISTICS

Throat Inches	ARC VOLTS kilogauss 1	2	4	8	16	20
Isp, sec 1000						
0.125	37.0	39.0	40.5	50.5	63.0	65.0
0.25	34.0	33.0	57.0	75.0	+	+
0.5	32.0	46.0	56.0	81.0	139	144
1.0	61.0	69.0	90.0	190	217	222
2.0						
Isp, sec 2000						
0.125	-	-	40.0	47.0	56.0	63.0
0.25	28.0	32.0	53.0	68.0	+	+
0.5	33.0	41.5	49.0	75.0	98.0	145
1.0	43.0	55.0	92.0	127	220	-
2.0						
Isp, sec 4000						
0.125						
0.25	-	-	52.0	69.0	+	+
0.5	37.0	40.0	50.0	73.0	104	117
1.0	46.0	62.0	91.0	131	-	-
2.0						
Isp, sec 8000						
0.125						
0.25						
0.5	-	-	54.0	70.0	97.0	105
1.0	78.0	90.0	148	148	-	-
2.0						

L/D = 1.5

TABLE 4

MEASURED CURRENT CHARACTERISTICS

Throat Inches	ARC AMPS kilogauss 1	2	4	8	16	20
Isp, sec 1000						
0.125	210	190	180	150	115	108
0.25	190	180	102	70	+	+
0.5	330	230	185	123	67	58
1.0	200	140	120	56	54	50
2.0						
Isp, sec 2000						
0.125	-	-	326	275	236	210
0.25	560	530	245	206	+	+
0.5	650	486	365	210	200	110
1.0	520	395	245	210	78	-
2.0						
Isp, sec 4000						
0.125						
0.25	-	-	460	370	+	+
0.5	1050	890	620	408	310	278
1.0	905	720	425	298	-	-
2.0						
Isp, sec 8000						
0.125						
0.25						
0.5	-	-	1180	850	680	609
1.0	1315	1185	575	570	-	-
2.0						

L/D = 1.5

TABLE 5

TOTAL POWER INPUT TO THE ARC

Throat Inches	KW INPUT kilogauss 1	2	4	8	16	20
Isp, sec 1000						
0.125	7.7	7.4	7.3	7.6	7.3	7.0
0.25	6.5	5.9	5.8	5.2	+	+
0.5	10.5	10.6	10.4	10.0	9.3	8.3
1.0	12.2	9.7	10.8	10.6	11.7	11.1
2.0						
Isp, sec 2000						
0.125	-	-	13.0	12.9	13.2	13.2
0.25	15.7	17.0	13.0	14.0	+	+
0.5	21.4	20.2	17.9	15.7	19.6	16.0
1.0	22.4	21.7	22.6	26.7	17.2	-
2.0						
Isp, sec 4000						
0.125						
0.25	-	-	-	23.9	25.5	+
0.5	38.9	35.6	31.0	29.8	32.3	32.5
1.0	41.7	44.6	38.7	39.0	-	-
2.0						
Isp, sec 8000						
0.125						
0.25						
0.5	-	-	63.7	59.4	65.9	63.9
1.0	103	107	85.0	84.3	-	-
2.0						

L/D = 1.5

TABLE 6

POWER IN THE GAS

Throat Inches	KW GAS kilogauss 1	2	4	8	16	20
Isp, sec 1000						
0.125	3.7	3.5	3.6	3.9	3.5	3.5
0.25	2.4	2.2	2.9	2.5	+	+
0.5	3.5	3.6	3.7	4.7	5.5	5.2
1.0	4.5	3.5	3.8	4.8	7.0	6.4
Isp, sec 2000						
0.125	-	-	6.8	7.2	7.3	7.8
0.25	8.3	9.5	7.0	7.9	+	+
0.5	12.0	10.3	8.5	9.0	9.5	10.6
1.0	13.0	12.0	10.0	10.0	8.7	-
2.0						
Isp, sec 4000						
0.125						
0.25	-	-	-	16.0	15.0	+
0.5	22.0	21.0	14.5	13.7	17.6	17.0
1.0	23.5	21.0	17.5	18.5	-	-
2.0						
Isp, sec 8000						
0.125						
0.25						
0.5	-	-	40.0	34.0	39.0	38.0
1.0	57.0	58.0	42.0	42.0	-	-
2.0						

L/D = 1.5

TABLE 7

THERMAL EFFICIENCY COMPUTED FROM TOTAL POWER AND GAS POWER MEASUREMENTS

Throat Inches	EFFICIENCY η^{eg}% kilogauss					
	1	2	4	8	16	20
Isp, sec 1000						
0.125	48	47	49	51	48	50
0.25	37	37	50	48	+	+
0.5	33	34	35	47	59	63
1.0	37	36	34	45	60	58
2.0						
Isp, sec 2000						
0.125	-	-	52	56	55	59
0.25	53	56	54	56	+	+
0.5	58	51	47	57	48	66
1.0	58	55	48	37	50	-
2.0						
Isp, sec 4000						
0.125						
0.25	-	-	-	67	59	+
0.5	56	59	47	46	54	52
1.0	55	47	45	47	-	-
2.0						
Isp, sec 8000						
0.125						
0.25						
0.5	-	-	63	57	59	60
1.0	55	54	49	50	-	-
2.0						

L/D = 1.5

TABLE 8

THRUST EFFICIENCY COMPUTED FROM GAS POWER, MASS FLOW AND THRUST MEASUREMENTS

Throat Inches	EFFICIENCY η^{gk}% kilogauss					
	1	2	4	8	16	20
Isp, sec 1000						
0.125	13.0	13.7	13.3	12.3	13.7	13.7
0.25	20.0	21.8	16.5	19.2	+	+
0.5	13.7	13.3	13.0	10.2	8.7	9.2
1.0	10.7	13.7	12.6	10.0	6.9	7.5
2.0						
Isp, sec 2000						
0.125	-	-	28.2	26.7	26.3	24.6
0.25	23.1	20.2	27.4	24.3	+	+
0.5	16.0	18.6	22.6	21.3	20.2	18.1
1.0	14.8	16.0	19.2	19.2	22.1	-
2.0						
Isp, sec 4000						
0.125						
0.25	-	-	-	48.0	51.2	+
0.5	34.9	36.6	53.0	56.0	43.7	45.2
1.0	32.7	36.6	43.9	41.6	-	-
2.0						
Isp, sec 8000						
0.125						
0.25						
0.5	-	-	76.9	91.0	78.7	80.7
1.0	53.8	52.9	73.0	73.0	-	-
2.0						

L/D = 1.5

When all four specific impulse values are completed a new series of electrodes is connected in place and a new series of tests start. Sometimes to obtain the complete data for a single geometry, various identical series of electrode geometries are needed because of premature failures. Sometimes, as shown in the tables, some conditions are too marginal, and in this case the relative data are not recorded. As shown in more detail in the following sections, the wide range of tests planned have the scope to discover the origin of anomalies detected or suspected in some results, especially at very low mass flow rate and pressure. The impossibility of producing real space conditions in the laboratory makes this work very difficult. It is believed that through an intensive and relatively wide series of experimental analyses some concrete results can be obtained.

A few remarks may be helpful in understanding the data in the various tables. Table 2 shows the arc chamber pressure in the various operating conditions. When a cross is in the place of a number, this indicates that the test is possible but has not been made. When a dash is in place of a number, this indicates that the particular test point is marginal and cannot be done.

It is evident from the table that the arc chamber pressure slightly decreases as the intensity of the magnetic field increases. As pointed out before, this data on the arc pressure may not be reliable due to the exaggerated length of the pressure gauge connections. Another factor that can affect the chamber pressure is the variation of the throat diameters due to erosion of the electrodes during the tests, especially when the possibility of

operation is marginal. For example, the variation of the pressure is inversely proportional to the throat area for the two larger diameters but is less than this for the two smaller diameters. This suggests that during operation the original diameter of the throat has been increased through erosion. For this reason, in all future tests it has been decided to measure the throat diameter after each run and to repeat this first series using this same precaution. Table 3 shows the variation of voltage and shows that the arc voltage increases with the intensity of the magnetic field and with throat diameter and that the ratio of increase with magnetic field is higher at the higher throat diameters. Table 4 shows the behavior of the arc current. Table 5 shows the behavior of the total input power and makes it evident that as the throat diameter is increased more power is necessary to produce the same I_{sp}, while increasing the magnetic field causes the reverse situation. Sometimes (as in the last line of the table) changing the magnetic field intensity from 2 to 4 kilogauss causes an abrupt, large decrease in the power input. This, we suggest, might be the onset of anomalies in the measurements. A similar change, relative to the total power in the gas, is put in evidence in Table 6. It is interesting to note that the thermal efficiency (Table 7) is only slightly affected by this condition, while the thrust efficiency (Table 8) shows practically the same variation of power input.

2.3 Search for Parasitic Effects

In our past report (Reference *, page 156 - 158), various circumstances capable of introducing errors in the measurements were examined. The possibility of anomalous results due to these causes were considered during the tests. Numerous and often complicated setups have been developed to clarify the mechanism of the suspected incorrect results. Unfortunately, at the present state of the work the anomalies have yet to be identified in a satisfactory and definite manner. In the early periods, the suspected effects were simply attributed to mechanical, thermal or magnetic interaction in the thrust measuring mechanism. For this reason various systems have been applied such as water-cooling, reduction of electromagnetic effects and elimination of thrust without interrupting the operation (thrust killer). With these modifications a few minor interactions have been discovered and eliminated. During this period of work various approaches have been taken to investigate the nature of other influences capable of giving erroneaous results in the measurement of the thrust values. Without illustrating in detail all the various approaches attempted, we will describe briefly those that seem deserving of further attention.

The system adopted recently to record simultaneously the arc picture and the values of the principal parameters of the test (as first mentioned in Section 2.3) is considered to be capable of interesting applications permitting a sort of "visual diagnostic" that might prove useful a long time after the experiment is over. Figures 17 to 36 show typical cases of arc operation in different conditions together with the principal operating values.

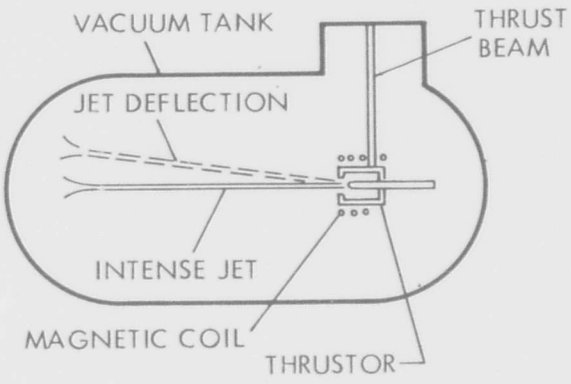

Figure 17. Schematic of Arc Exhaust at Low Power Input and Low Magnetic Field Strength Showing Unexplained Jet Deflection

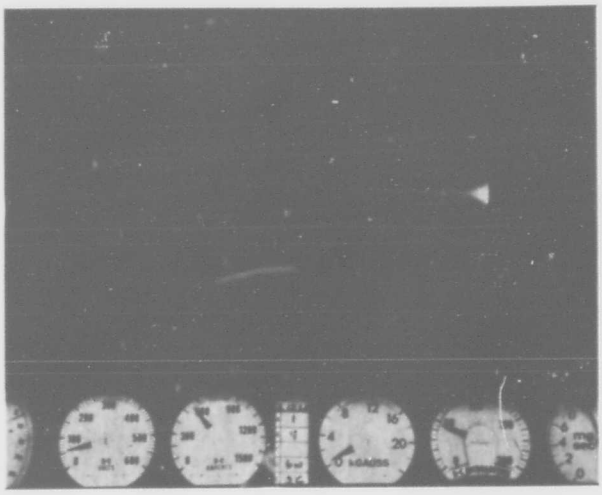

Figure 18. Photograph of Deflected Jet of Figure 17 With Simultaneous Recording of Test Instrumentation at Low Power Range and Approximate Specific Impulse of 2000 Seconds

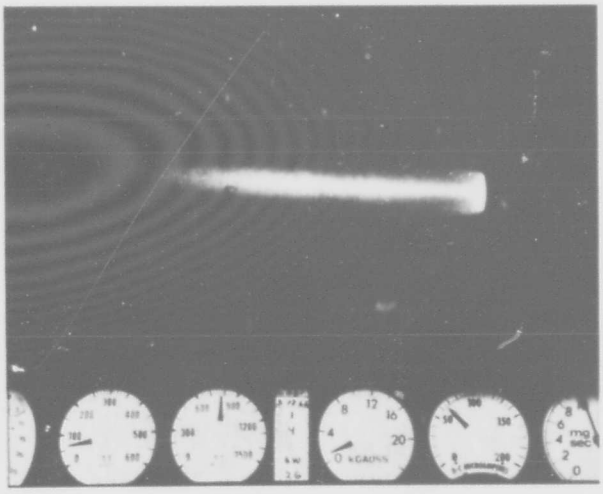

Figure 19. Photograph of Jet Similar to Figure 18 But Operating at Higher Specific Impulse Level

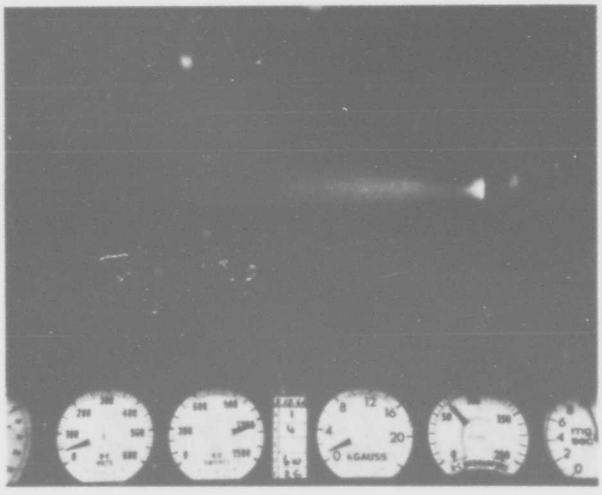

Figure 20. Photograph of Jet When the Arc Current is Increased Indicating a Transition in the Structure of the Plasma Exhaust

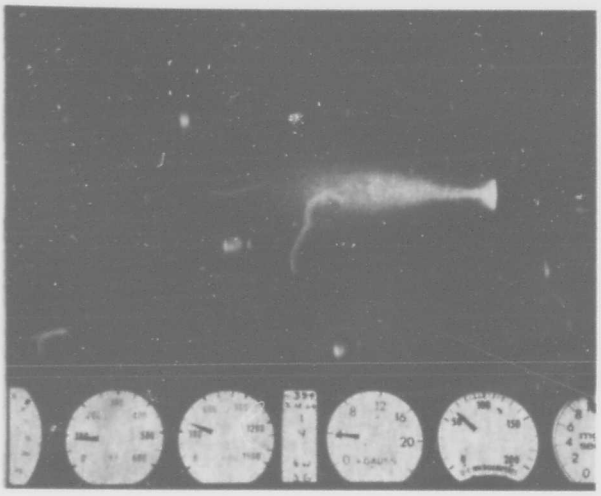

Figure 21. Photograph of Jet at Increased Magnetic Field Strength and Constant Power Input and Specific Impulse Level

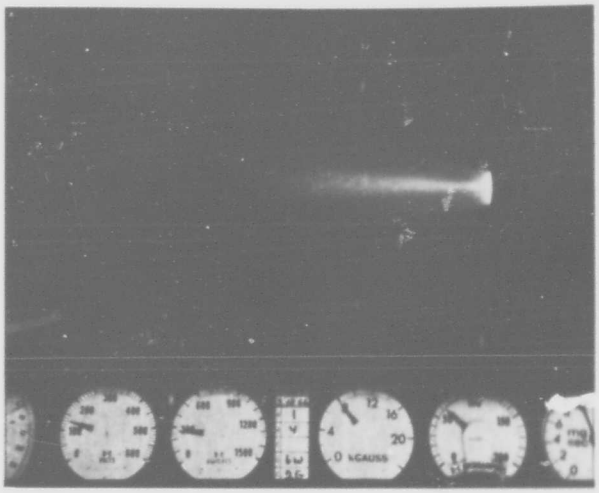

Figure 22. Photograph of Jet at Further Increased Magnetic Field and Constant Power Input Shows Distinct Formation of Center Core

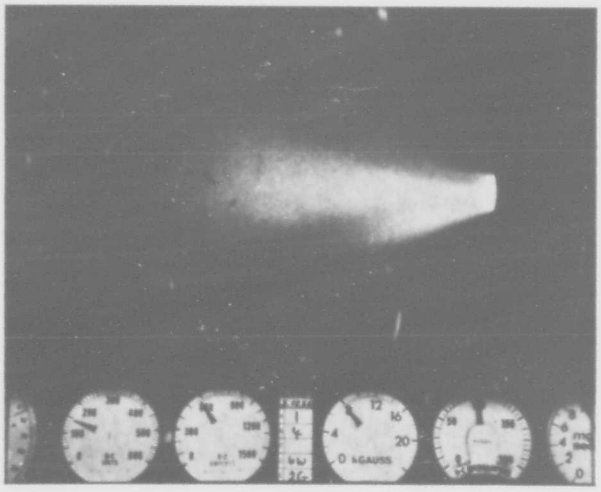

Figure 23. Photograph of Jet Showing a Separation of Inner Core From Outer Glow at Increased Input Power and Constant Magnetic Field

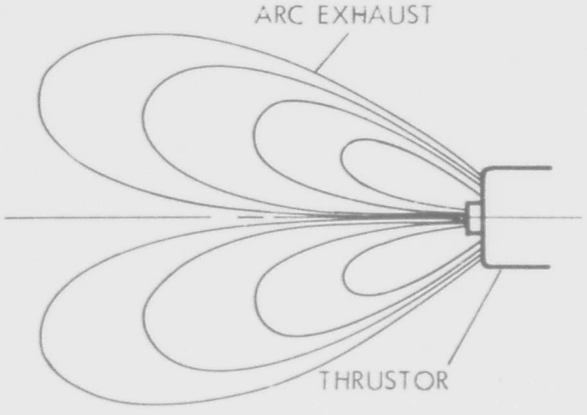

Figure 24. Schematic of Assumed Current Discharge Pattern of the Low Pressure Plasma Exhaust

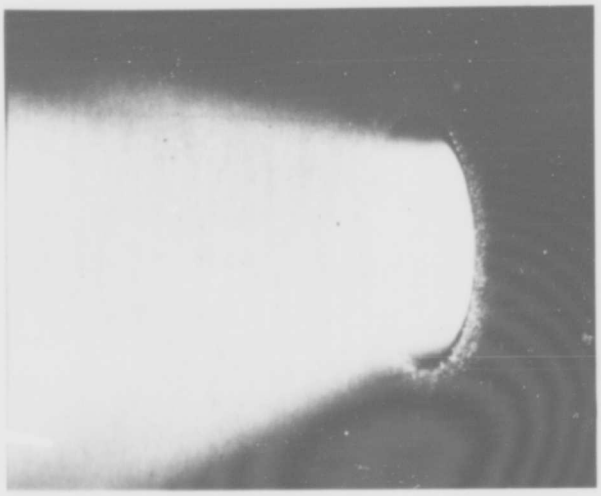

Figure 25. Photograph of Arc Exhaust Showing Distinct Luminous Area Apparently Caused by Electron Bombardment on Anode Surface

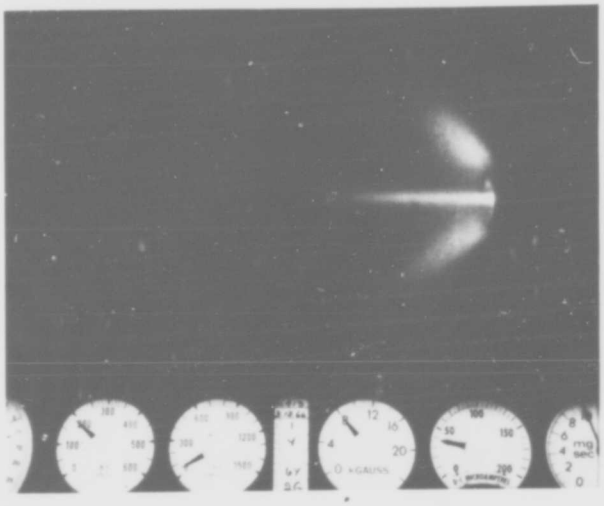

Figure 26. Photograph of Jet Similar to Figure 23 Showing Complete Separation of Inner Core From Outer Glow at Constant Magnetic Field and Reduced Input Power

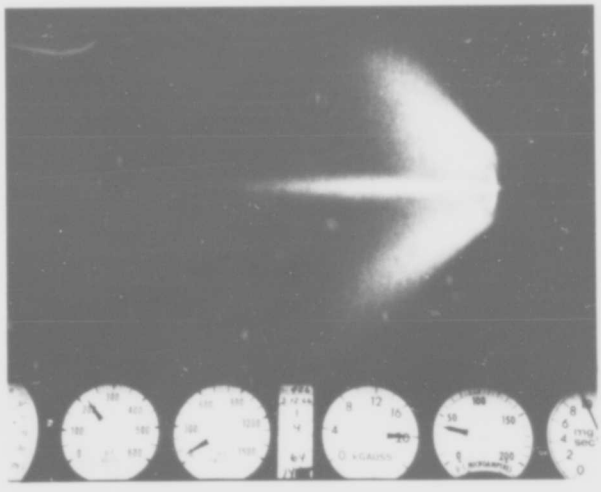

Figure 27. Photograph of Jet Similar to Figure 26 at Increased Magnetic Field and Reduced Input Power

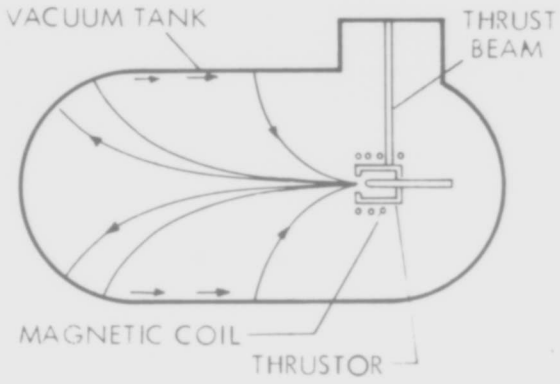

Figure 28. Schematic of Test Tank Showing Assumed Flow Discharge of Arc Plasma Along Magnetic Field Lines and Tank Walls

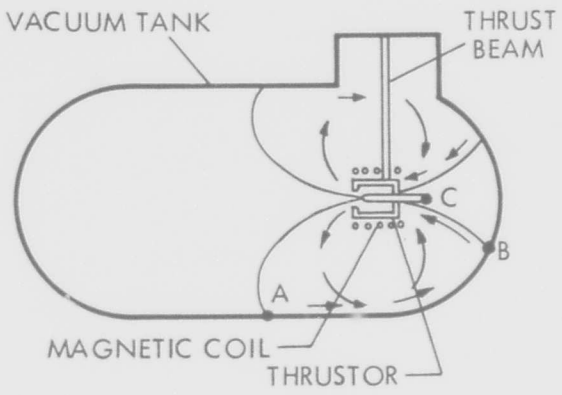

Figure 29. Schematic of Arc Plasma Patterns Showing Discharges to Test Tank Upstream and Downstream of Thrustor Along Magnetic Field Lines

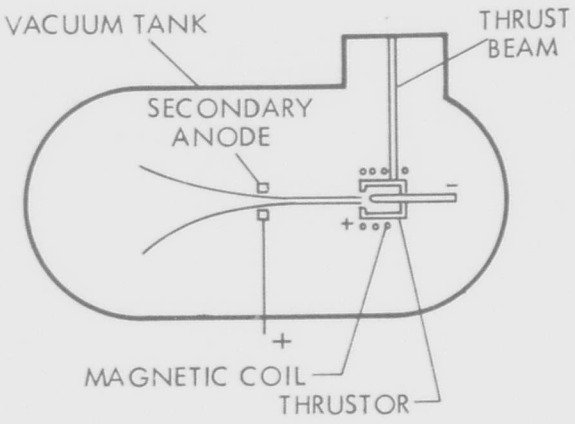

Figure 30. Schematic of Test Tank Showing Attachment of Secondary Anode Ring Downstream of Thrustor Anode

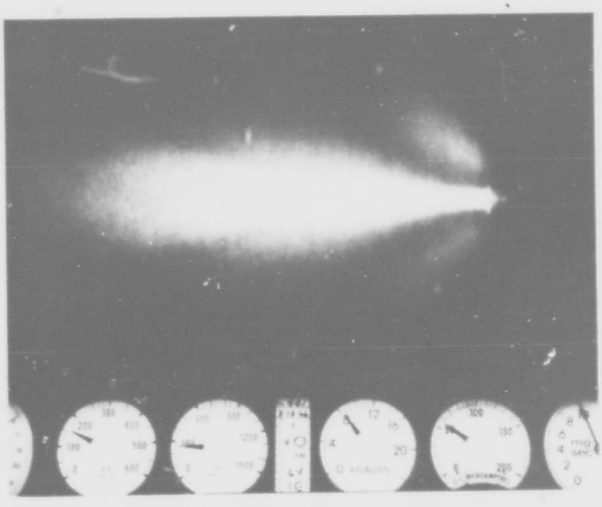

Figure 31. Photograph of Jet Showing Reduced Appearance of Separate Outer Glow Affected by Secondary Anode Attachment at Constant Power Input and Specific Impulse Level

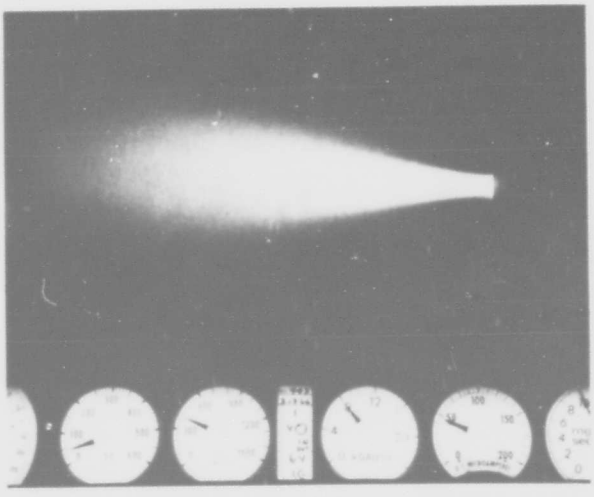

Figure 32. Photograph of Jet Showing Complete Elimination of Separate Outer Glow at Increased Voltage Potential to Secondary Anode

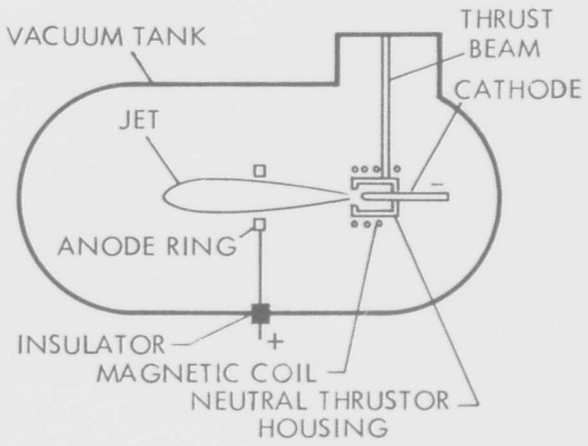

Figure 33. Schematic of Test Tank Showing Separate Anode Ring Attached Downstream of Thrustor Housing

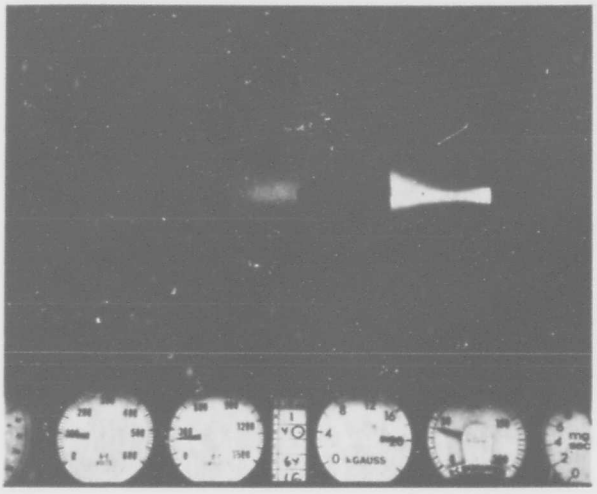

Figure 34. Photograph of Jet Without Outer Glow Obtained With Separate Anode Ring Downstream of Thrustor Housing at Constant Input Power and High Magnetic Field

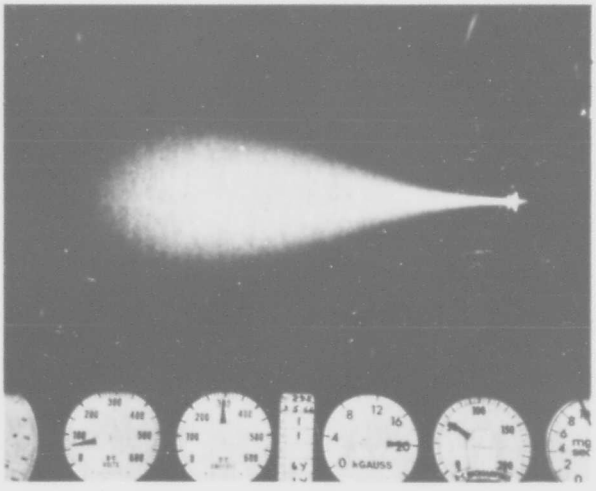

Figure 35. Photograph of Jet Obtained With a Small Throat Diameter and Large L/D Ratio Showing No Separate Outer Glow, at Very High Magnetic Field

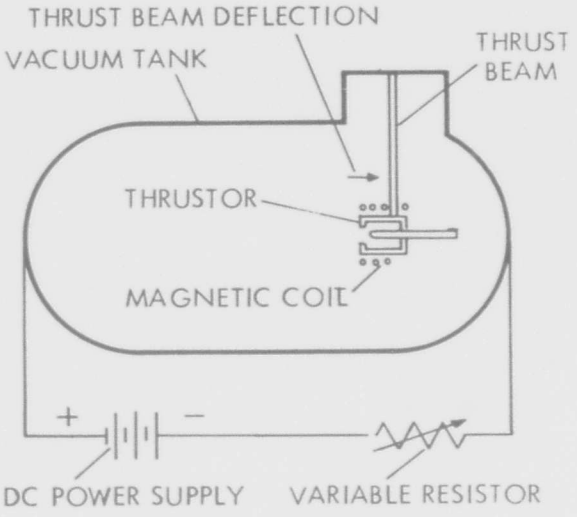

Figure 36. Schematic of Test to Detect Thrust Variation Due to Currents Flowing in Tank Walls

The black and white prints and the mediocre reproduction do not give the details of the original pictures, but show characteristic behavior, and have already been of some use. The arc jet pictures acquire typical aspects in dependence of the arc chamber pressure, throat diameter, magnetic field, specific impulse, and so forth. Particularly (and especially when color is reproduced), the pictures have been very useful to show the behavior of the external part of the arc and to advance ideas on its probable effects on the thrust measurements. The interpretation of the pictures will require a long time, but some images are already quite "typical" and may induce different suggestions to various experimenters. For this reason it may be useful to describe in detail the twenty pictures mentioned above (Figures 17 to 36).

Visually, the most conspicuous part of any plasma jet is the central core which generally exhibits the highest temperature and luminosity and protrudes in the vacuum chamber on a straight line along the axis of the plasma generator. This luminous, straight center core is generally surrounded by a glow of variable intensity and of geometrical form which depends on the operating conditions. The visual recordings that we are now planning to illustrate are relative to the above mentioned center core and the variable aspects of its surrounding glow. For simplicity of description we start from an arbitrary initial condition and particularly from a condition of relatively low enthalpy of the gas (or low specific impulse). Schematically, in this case, the jet appears as a long, uniform, straight line emanating from the throat of the plasma generator and fading out along the vacuum chamber as illustrated in Figure 17. Often this line is not

symmetrical with the axis of the tank, but inclined (dotted line) in a direction that might vary sometimes but remains stable for any particular set of experimental conditions. Figure 18 is an actual photograph of this particular aspect of the jet. This is obtained with a double image camera that records simultaneously the arc jet and the principal instruments. From left to right the first instrument reads the arc chamber pressure in millimeters (Torr), the second the arc voltage in volts, the third the arc current in amperes, the fourth the magnetic field intensity in kilogauss, the fifth the thrust in arbitrary units, the sixth the mass flow in milligrams per second. At the center, a small table that is changed in each test indicates the date, the propellant, the throat size, and photographic and other miscellaneous data. In the present state of our experiments it is not clear if this long rectilinear path of the jet and its eventual stable inclination is due to a direct discharge to the vacuum tank or to other reasons (like the geometry of the arc chamber and electrodes). The first hypothesis is preferred in our laboratory, but further experiments are necessary to confirm it, especially if insulated vacuum chambers are available in the future. In Figure 18 the jet (commonly called the cathode jet) is inclined in respect to the axis of the tank and is uniformly luminous for several feet along the tank. In this particular picture a throat diameter of one inch was used with a mass flow of 10 mg/sec and with a small external magnetic field (about 250 gauss). The arc voltage is low (60 volts) and the arc current relatively high (400 to 500 amps). Figure 19 shows a similar straight jet operating always at very low external magnetic field but with increased input power. While a coaxial glow surrounds the jet, the inclination and

direction remains the same. The long straight line form of this particular jet and the preferred direction to one point seems to indicate the presence of some anomalies. For these reasons, further study of these experimental conditions, especially with and without insulated tanks, might provide some useful information.

Figure 20 shows the interesting transition between the straight inclined jet and a horizontal symmetrical jet. With an increase of the arc current, the voltage drops, the total power remains the same and the jet shortens and fattens acquiring normal proportions. Increasing the magnetic field (from 500 to 4000 gauss), the current decreases and the voltage increases, again in proportion, but the jet maintains and also improves its regular form while input power and specific impulse remain unvaried as illustrated in Figure 21. The central part of the jet increases its luminosity while the outside part glows more and more. Increasing the magnetic field from 4 to 8 kilogauss and maintaining the same specific impulse, the arc voltage increases and the current decreases (as in Figure 22) and the core of the jet becomes more concentrated and luminous, apparently beginning a separation from the outside glow. At this point an increase in power input produces a net separation between the inner core and the outside glow as illustrated in Figure 23. A similar appearance is obtained at the same input power with only an increase of the magnetic field. Figure 24 shows schematically the estimated process that is taking place in the space outside the arc chamber, and that, because of the presence of the metal environment, is supposed to introduce some anomalous results in the measurements.

With the net separation between the inner core and the outside glow and when the input power is relatively high, another important phenomenon is taking place. Where the external glow terminates to the anode some luminous spots appear and gradually multiply and enlarge as soon as the power is increased. The intensity of these spots is high enough to cause the melting of the anode even if the material is cooled. This phenomenon, better seen in an enlarged version in Figure 25, not only increases the thermal losses but also imposes a limit to the maximum power input to avoid dangerous effects or even destruction of the anode. The point where the bombardment spots are beginning to be produced is very sharp and slight variation of power input and/or magnetic field can produce or eliminate them. It is anticipated that the programmed future experiments with higher ratios between throat lengths and diameters will supply important information along this line. Due to the sharpness of the onset of the electron bombardment of the anode it is relatively easy to prevent the bombardment by controlling the power input, the magnetic field or the geometry of the thrustor.

By reducing the power input of Figure 23 and maintaining a constant magnetic field (8 kilogauss), the pictures of Figures 26 and 27 are obtained which show a complete separation between the inner core and the outside glow. The presence of the metal vacuum tank suggests, in this case, that the central core discharges at the end of the tank and the return path of the current progresses along the tank walls until a new discharge is produced to complete the path to the anode as illustrated in Figure 28. This second discharge is shaped along the magnetic field lines generated by the coil

placed around the thrustor. It is noted that when these conditions are reached the connections to the anode in the back of the vacuum tank begin to glow with an intensity which increases with the power input and the magnetic field until, at a certain point, a real outside arc is started. The discharge always happens between points A, B and C of Figure 29. While a precise explanation of these discharges is not elaborated, it seems that they are following the symmetrical lines of the magnetic field in front and in back of the arc chamber. The possibility that under these conditions relatively strong currents might circulate in the tank with magnetic interactions capable of producing parasitic thrust forces is another effect to be investigated in the search for anomalies.

To eliminate the discharge to the tank, a secondary positive electrode has been located downstream as schematically illustrated in Figure 30. With a slightly positive overvoltage applied to this electrode the separate outside glow (wings) is reduced in dimension (Figure 31). By increasing the positive voltage of this secondary electrode a point is reached where the outside glow disappears completely (Figure 32). While the specific impulse remains practically unchanged, the main anode voltage drops and the main arc current increases. The effect of this secondary electrode on the other parameters of the plasma jet will be investigated in the next period. Following and developing this idea, the complete anode, constituted by a ring of wide diameter has been put downstream in the tank as schematically illustrated in Figure 33. A regular jet without side glow has been obtained as shown in the picture of Figure 34, but the effect on the thrust value has not been investigated at the end of this period.

It is evident that further investigation on the outside part of the jet is necessary with the goal of the development of a plasma jet which is independent of the environmental conditions. Experiments with secondary electrodes and/or higher length to diameter ratios as planned for the next period will probably give new data on this important matter. Figure 35 is a picture of a jet without side lobes obtained with a long, small diameter throat and very high external magnetic field. We have considered the possibility that a similar combination of a strong magnetic constriction with a downstream anode may limit the interaction of the arc with the environment; an investigation of this configuration has been planned. From the examination of many of the test pictures the possible effects of the external part of the jet on the measured values appears important. When a net separation exists between cathode and anode jets (as illustrated in Figures 24, 26 and 27), the possibility of anomalous results seems to increase. This has suggested that in these cases, direct discharges to the test tanks are present with the conduction of substantial currents in their walls. An artificial d.c. current in the test tank walls, as illustrated in Figure 36, causes a deflection of the thrust stand. Further tests are necessary to prove the importance of the interaction of tank currents on the thrust readings. As recommended some time ago, the use of a tank with insulating walls would eliminate this inconvenience.

During the following period tests using a secondary insulating tank will be conducted. When the experimental data includes all the geometries, the photographic material will be extended to a larger number of conditions, especially on the effect of the throat length on the expanded plasma jet and

its interaction with the environment. The study of gas entrainment or recirculation of gas in the testing tank has been approached by changing the residual pressure in the test chamber from 5 to 200 Torr, but no measurable effect has been detected. Tests at vacuum levels many orders of magnitude higher are necessary to have a probability of success in this analysis. For this reason, testing tanks made of insulating materials and operating at extremely low pressures seem to be very important to a successful continuation of the investigation on the anomalous results.

3.0 EFFICIENCY STUDY

The complete test data is presented in Table 9. The various electrode configurations used are shown in Figures 9 and 10. The arc jets were tested over a 1000 to 8000 second specific impulse range while employing applied magnetic fields up to 20 kilogauss (see Figure 37). The data has been recorded during steady and stable operation and thus represents steady state performance. Each entry in Table 9 is an average over several distinct tests.

Mass flow, thrust, total electrical power to the jet (not including magnetic coil and circuit losses), power to electrode cooling water and power to the vacuum tank walls have been directly measured. The specific impulse is computed from

$$I_{sp} = \frac{F}{\dot{m}} \qquad (1)$$

where F and $\dot{m}$ are the measured thrust and mass flow rate. The specific impulse calculated from (1) is subject to the criticism that under some conditions one is not sure what value of the mass flow to use. Of course, it would be desirable to measure the velocity and mass density profile to compute the specific impulse. The chamber pressure has been measured at the position indicated in Figure 38.

The thermal efficiency is denoted by η^{eg} and represents the effectiveness of the transfer of electrical power to power in the gas. The power in the gas is the total electrical power input P minus the power loss to the

Throat Inches	ARC PRESSURE MM						ARC VOLTS						ARC AM			
	kilogauss						kilogauss						kilogau			
	1	2	4	8	16	20	1	2	4	8	16	20	1	2	4	
Isp, sec 1000																
0.125	156	154	152	150	142	+	37.0	39.0	40.5	50.5	63.0	65.0	210	190	180	1
0.25	36.0	37.0	31.0	28.0	+	+	34.0	33.0	57.0	75.0	+	+	190	180	102	
0.5	26.0	24.6	23.5	21.5	18.9	19.0	32.0	46.0	56.0	81.0	139	144	330	230	185	1
1.0	7.3	7.0	6.6	7.0	7.0	6.5	61.0	69.0	90.0	190	217	222	200	140	120	
2.0																
Isp, sec 2000																
0.125	-	-	190	198	194	190	-	-	40.0	47.0	56.0	63.0	-	-	326	2
0.25	48.0	52.0	40.0	38.0	+	+	28.0	32.0	53.0	68.0	+	+	560	530	245	2
0.5	27.0	26.0	25.0	23.0	24.0	20.5	33.0	41.5	49.0	75.0	98.0	145	650	486	365	2
1.0	6.5	6.0	4.0	4.5	5.5	-	43.0	55.0	92.0	127	220	-	520	395	245	2
2.0																
Isp, sec 4000																
0.125																
0.25	-	-	50.0	48.0	+	+	-	-	52.0	69.0	+	+	-	-	460	3
0.5	-	31.0	28.0	25.8	25.6	26.0	37.0	40.0	50.0	73.0	104	117	1050	890	620	4
1.0	7.5	7.5	4.8	4.5	-	-	46.0	62.0	91.0	131	-	-	905	720	425	2
2.0																
Isp, sec 8000																
0.125																
0.25																
0.5	-	-	29.0	29.5	28.5	27.5	-	-	54.0	70.0	97.0	105	-	-	1180	8
1.0	-	6.7	7.5	7.5	-	-	78.0	90.0	148	148	-	-	1315	1185	575	5
2.0																

C AMPS				KW INPUT						KW GAS						EFFICIENCY			
logauss				kilogauss						kilogauss						kilogaus			
4	8	16	20	1	2	4	8	16	20	1	2	4	8	16	20	1	2	4	8
80	150	115	108	7.7	7.4	7.3	7.6	7.3	7.0	3.7	3.5	3.6	3.9	3.5	3.5	48	47	49	51
02	70	+	+	6.5	5.9	5.8	5.2	+	+	2.4	2.2	2.9	2.5	+	+	37	37	50	48
85	123	67	58	10.5	10.6	10.4	10.0	9.3	8.3	3.5	3.6	3.7	4.7	5.5	5.2	33	34	35	47
20	56	54	50	12.2	9.7	10.8	10.6	11.7	11.1	4.5	3.5	3.8	4.8	7.0	6.4	37	36	34	45
26	275	236	210	-	-	13.0	12.9	13.2	13.2	-	-	6.8	7.2	7.3	7.8	-	-	52	56
45	206	+	+	15.7	17.0	13.0	14.0	+	+	8.3	9.5	7.0	7.9	+	+	53	56	54	56
65	210	200	110	21.4	20.2	17.9	15.7	19.6	16.0	12.0	10.3	8.5	9.0	9.5	10.6	58	51	47	57
45	210	78	-	22.4	21.7	22.6	26.7	17.2	-	13.0	12.0	10.0	10.0	8.7	-	58	55	48	37
60	370	+	+	-	-	-	23.9	25.5	+	-	-	-	16.0	15.0	+	-	-	-	67
20	408	310	278	38.9	35.6	31.0	29.8	32.3	32.5	22.0	21.0	14.5	13.7	17.6	17.0	56	59	47	46
25	298	-	-	41.7	44.6	38.7	39.0	-	-	23.5	21.0	17.5	18.5	-	-	55	47	45	47
180	850	680	609	-	-	63.7	59.4	65.9	63.9	-	-	40.0	34.0	39.0	38.0	-	-	63	57
75	570	-	-	103	107	85.0	84.3	-	-	57.0	58.0	42.0	42.0	-	-	55	54	49	50

B

TABLE 9

SUMMARY OF COMPLETE TEST DATA

EFFICIENCY η^{eg} %					EFFICIENCY η^{gk} %						EFFICIENCY η^{ek} %					
kilogauss					kilogauss						kilogauss					
2	4	8	16	20	1	2	4	8	16	20	1	2	4	8	16	20
47	49	51	48	50	13.0	13.7	13.3	12.3	13.7	13.7	6.2	6.5	6.6	6.3	6.6	6.9
37	50	48	+	+	20.0	21.8	16.5	19.2	+	+	7.4	8.1	8.3	9.2	+	+
34	35	47	59	63	13.7	13.3	13.0	10.2	8.7	9.2	4.6	4.5	4.6	4.8	5.2	5.8
36	34	45	60	58	10.7	13.7	12.6	10.0	6.9	7.5	3.9	4.9	4.7	4.5	4.1	4.3
-	52	56	55	59	-	-	28.2	26.7	26.3	24.6	-	-	14.8	14.9	14.5	14.5
56	54	56	+	+	23.1	20.2	27.4	24.3	+	+	12.2	11.3	14.8	13.7	+	+
51	47	57	48	66	16.0	18.6	22.6	21.3	20.2	18.1	8.9	9.5	10.7	12.2	9.8	12.0
55	48	37	50	-	14.8	16.0	19.2	19.2	22.1	-	8.6	8.8	8.5	7.2	11.2	-
-	-	67	59	+	-	-	-	48.0	51.2	+	-	-	-	32.1	30.1	+
59	47	46	54	52	34.9	36.6	53.0	56.0	43.7	45.2	19.8	21.6	24.8	25.8	23.8	23.6
47	45	47	-	-	32.7	36.6	43.9	41.6	-	-	18.4	17.2	19.8	19.7	-	-
-	63	57	59	60	-	-	76.9	91.0	78.7	80.7	-	-	48.2	51.6	46.6	48.1
54	49	50	-	-	53.8	52.9	73.0	73.0	-	-	29.8	28.7	36.1	36.1	-	-

C

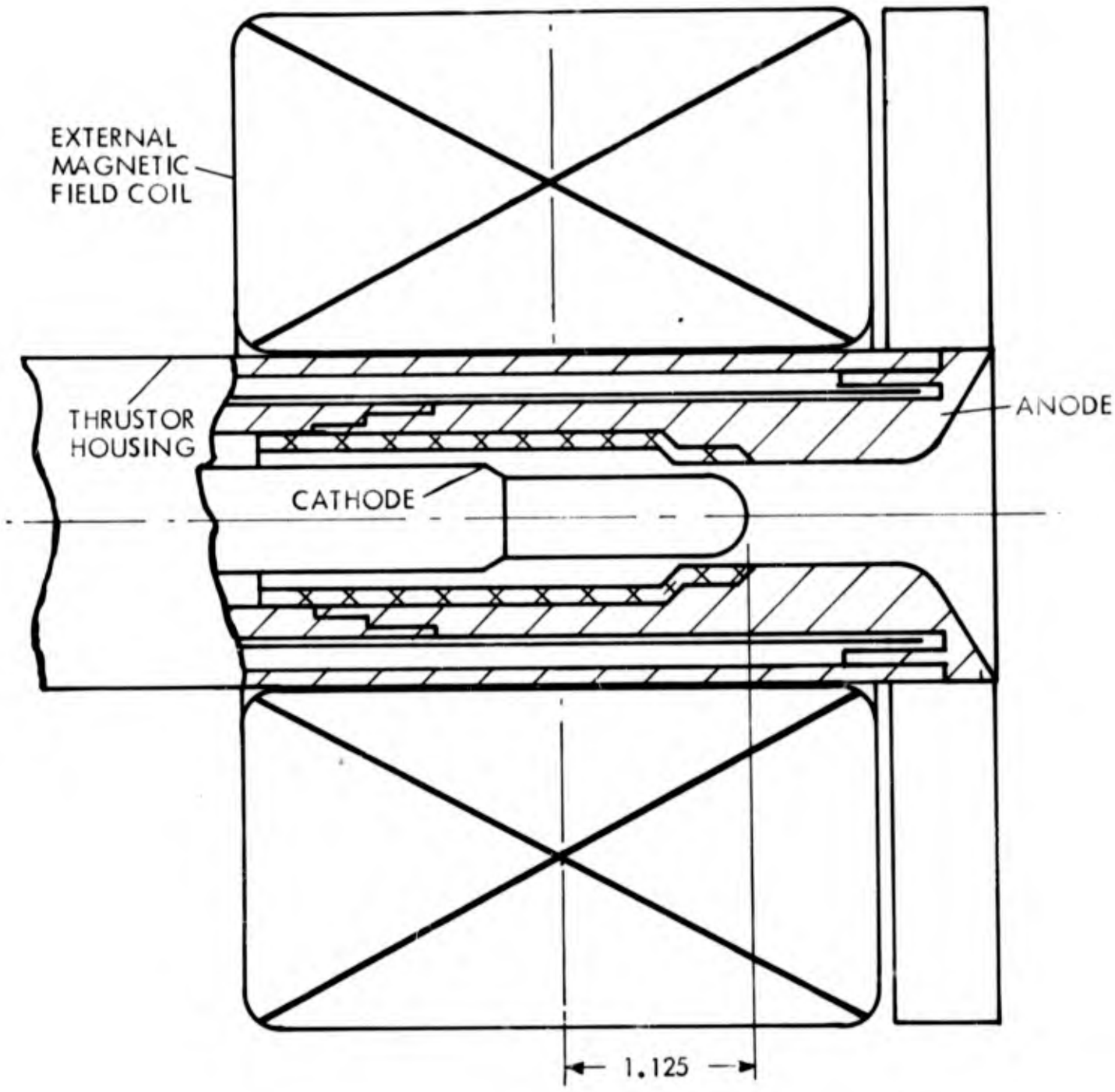

Figure 37. Schematic of Electrode Configuration Showing Position With Respect to Magnetic Field Coil

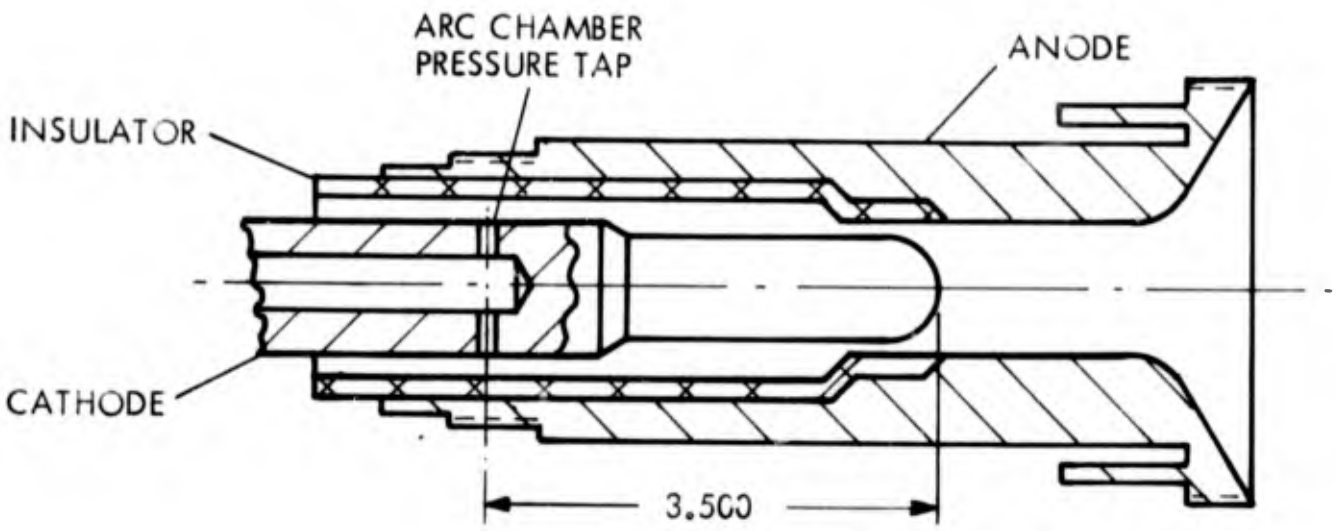

Figure 38. Schematic of Electrode Configuration Showing Position of Arc Chamber Pressure Tap

electrodes and arc chamber. The thermal efficiency is defined as

$$\eta^{eg} = \frac{\text{Power in gas}}{P} . \qquad (2)$$

The thrust efficiency η^{gk} is the efficiency of the recovery of the gas power in the form of directed kinetic energy of the jet and is given by

$$\eta^{gk} = \frac{\text{Thrust power}}{\text{Power in gas}} = \frac{F^2/2\,\dot{m}}{\text{Power in gas}} . \qquad (3)$$

The overall efficiency is given by

$$\eta^{ek} = \frac{F^2}{2\,\dot{m}\,P} \qquad (4)$$

and according to (2) and (3)

$$\eta^{ek} = \eta^{eg}\,\eta^{gk} . \qquad (5)$$

This manner of separating the total losses into thermal and expansion losses is generally used and has proved to be useful in understanding the performance characteristics of the arc jet.

3.1 Thermal Efficiency

Dependence of Thermal Efficiency on Magnetic Field Strength

Figures 39, 40, 41 and 42 show thermal efficiency as a function of magnetic field strength for four throat diameters at specific impulses of 1000, 2000, 4000, and 8000 seconds, over a 1 to 16 kilogauss range. At specific impulses equal to and larger than 2000 seconds and for a fixed throat diameter, the thermal efficiency is relatively insensitive to magnetic field strength. At 1000 seconds (Figure 39) the thermal efficiency for the 1/8-inch throat is very flat, while the data for the larger throats shows a definite increase with magnetic field strength. We note that the thermal efficiencies were about 60 percent or less for all I_{sp} and magnetic fields. The thermal efficiency shows a definite tendency to increase with decreasing throat size. We remark that the increase in thermal efficiency at 1000 seconds achieved by utilizing the magnetic field has also been approximately obtained by decreasing the throat diameter at a low magnetic field strength.

Dependence of Thermal Efficiency on Specific Impulse

Thermal efficiency is shown as a function of specific impulse in Figure 43 The experimental points shown have been obtained by taking the efficiency at the smallest throat used and then averaging the efficiencies over the different magnetic field strengths. A moderate increase in thermal efficiency occurs in the 1000 to 2000 second range, and it is approximately constant in the high specific impulse range. Our measurements thus

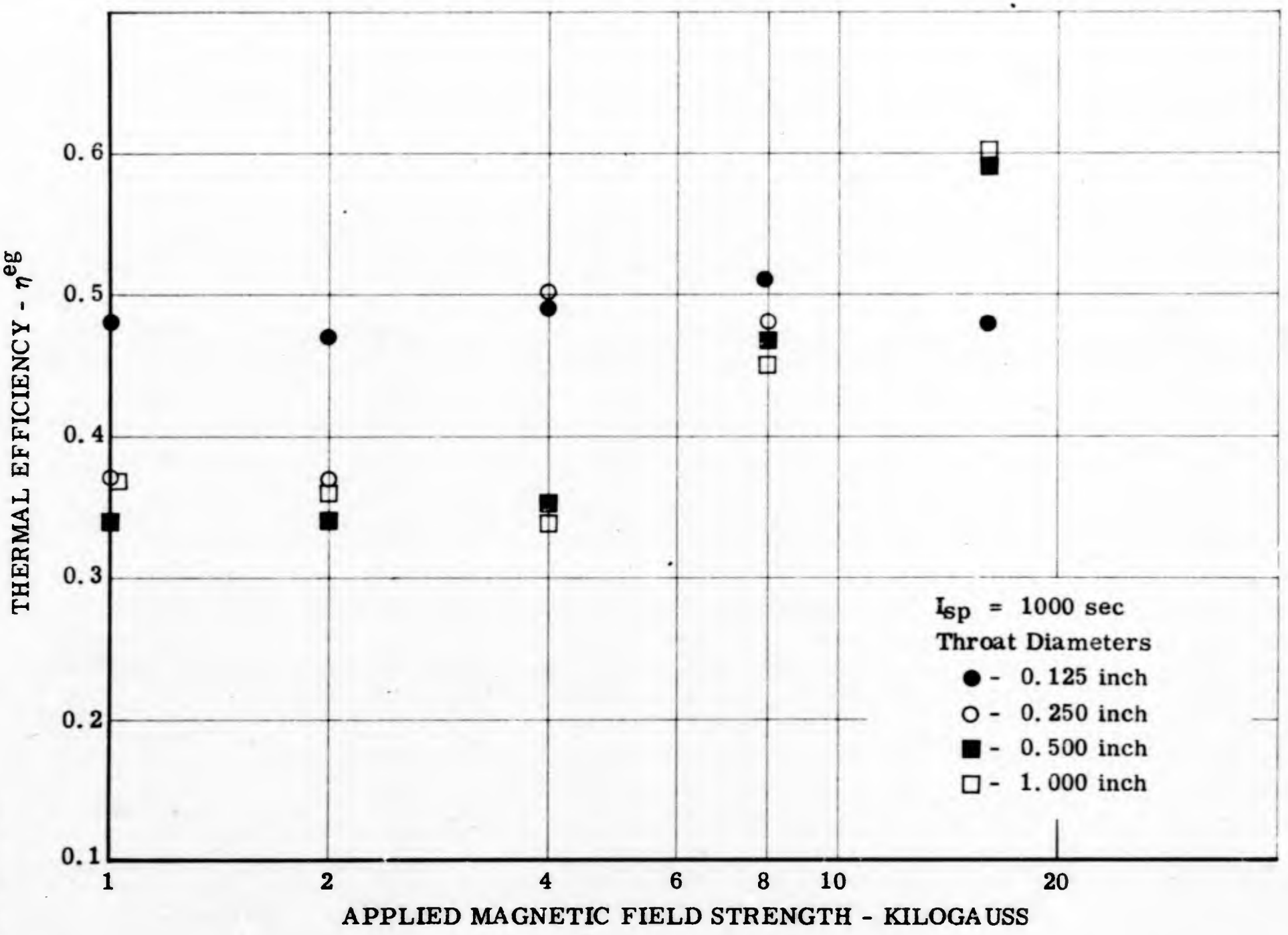

Figure 39. Thermal Efficiency as a Function of Magnetic Field Strength at Constant Specific Impulse

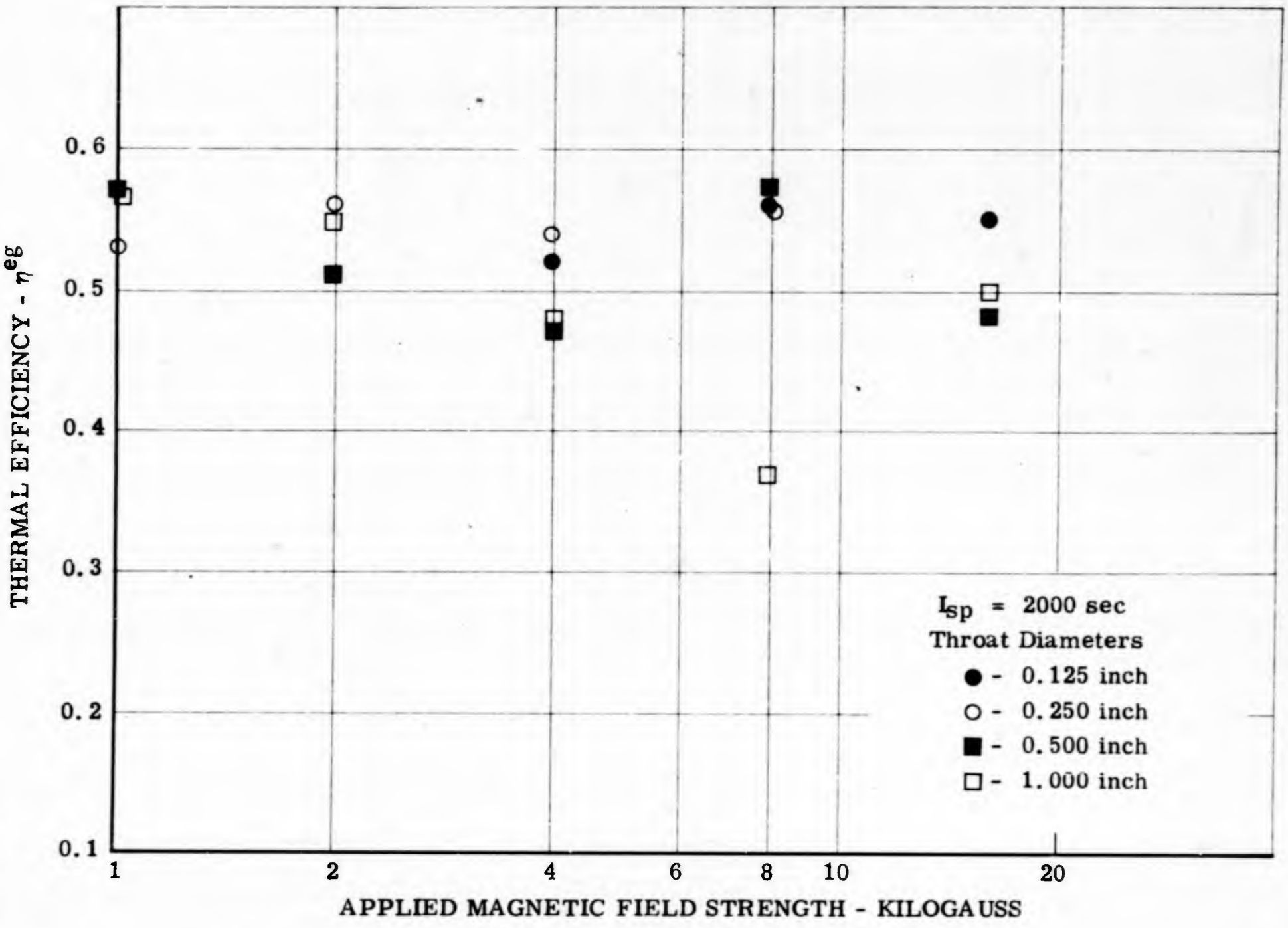

Figure 40. Thermal Efficiency as a Function of Magnetic Field Strength at Constant Specific Impulse

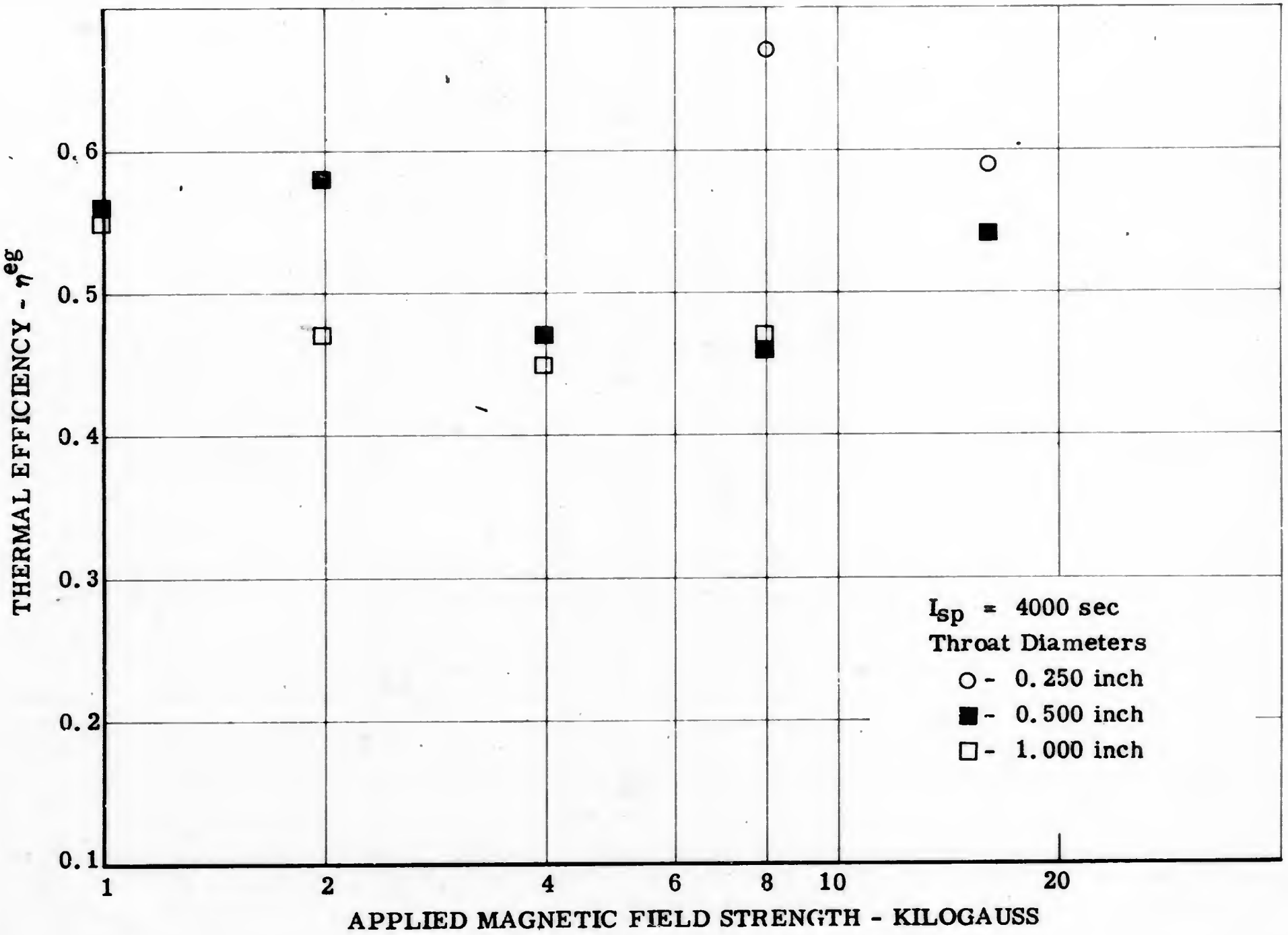

Figure 41. Thermal Efficiency as a Function of Magnetic Field Strength at Constant Specific Impulse

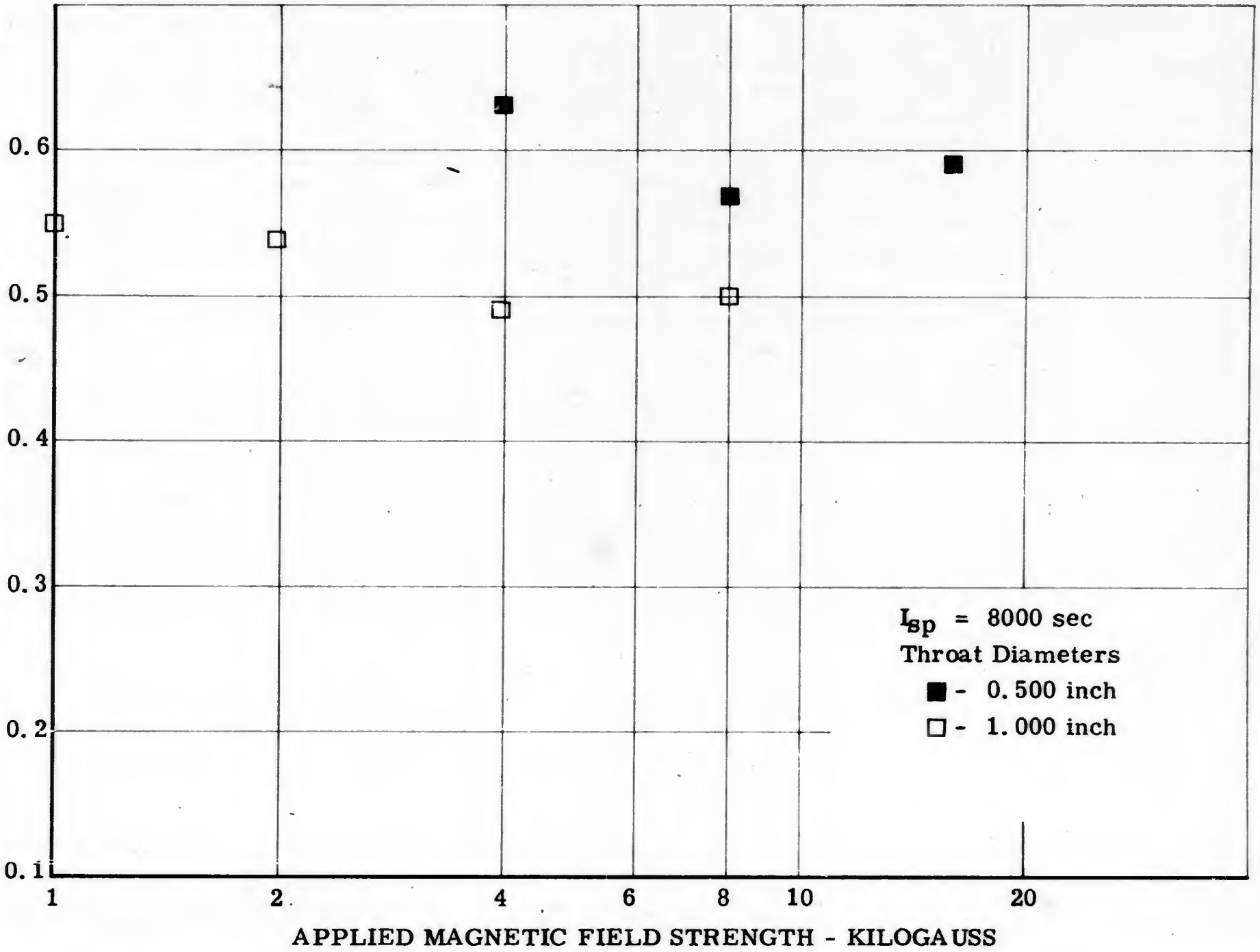

Figure 42. Thermal Efficiency as a Function of Magnetic Field Strength at Constant Specific Impulse

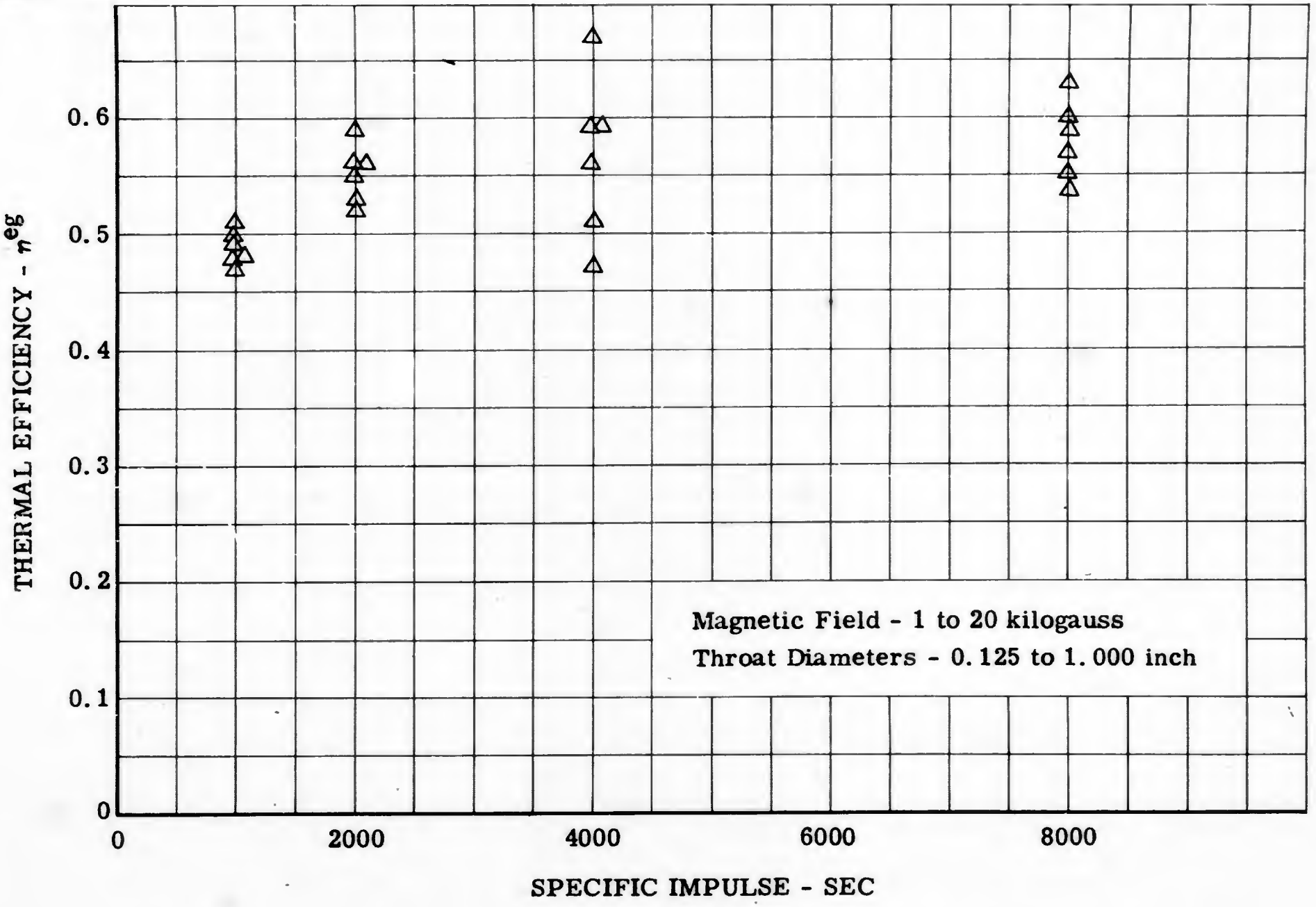

Figure 43. Thermal Efficiency as a Function of Specific Impulse for Smallest Throat Used at Each Magnetic Field Strength and Specific Impulse

show the thermal efficiency to be approximately independent of both magnetic field strength and specific impulse at specific impulses larger than 4000 seconds.

The voltage current characteristics of the arc are such that when the magnetic field strength is increased at approximately constant power the voltage goes up and the current goes down. The dependence of thermal efficiency on B and I_{sp} implies that the electrode power loss (the loss to the chamber is small) is approximately a linear function of the specific enthalpy of the flow and does not depend explicitly on voltage or current, but depends only on the power in the gas, in the high range of I_{sp}.

3.2 Thrust Efficiency

Dependence of Thrust Efficiency on I_{sp}

The measured thrust efficiency is shown in Figure 44. Each point is the average over the four throat diameters shown in Table 9. The thrust efficiency also shows a tendency to increase as the throat diameter decreases; however, we have plotted average values since they adequately represent the performance properties we shall discuss at this point. For clarity, points of equal specific impulse have been connected with straight lines.

In Figure 44, at 1000 seconds, the thrust efficiency is seen to be essentially independent of magnetic field strength. At 2000 seconds there is a definite, though small, increase between 2 and 4 kilogauss. A larger increase in efficiency between 2 and 4 kilogauss occurs at 4000 seconds. At 8000 seconds, in the same range of magnetic field strength, there is a very large increase in η^{gk}. Further increase in B beyond 4 kilogauss does not produce significant changes in the thrust efficiency.

The high efficiencies at 8000 seconds exceed the frozen flow efficiency by about 15 percent. These measurements imply that there exists spurious effects or else the flow is in a strongly nonequilibrium state with the ions more energetic than the electrons, or that there is appreciable recombination. Anomalously high thrust efficiencies obtained with arc jets have been attributed to the ingestion, heating and expansion of ambient gas,[2] to spurious interactions of the arc with the test tank and electrode vaporization.[1] The high efficiencies occur in a domain of high temperature and

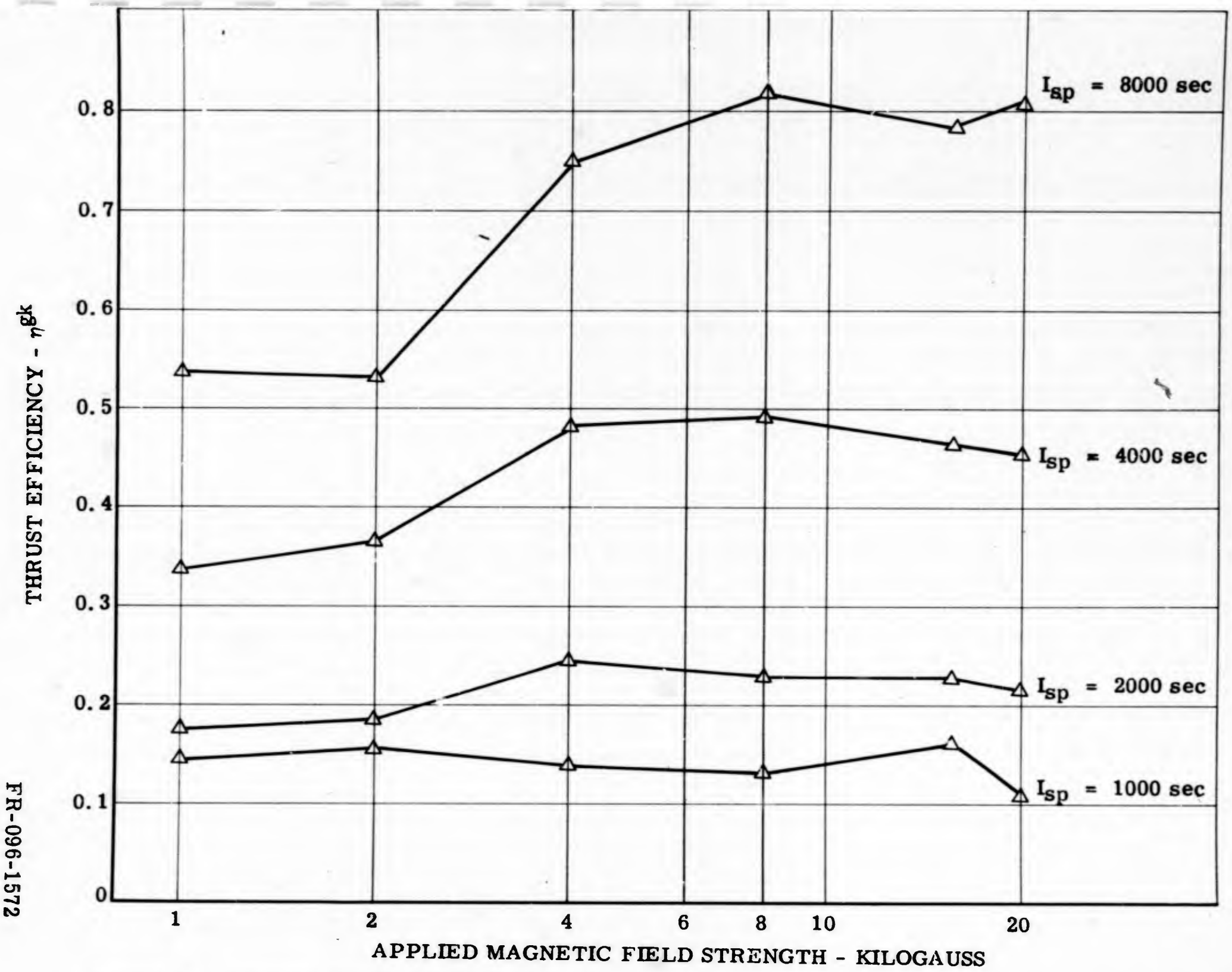

Figure 44. Average Thrust Efficiency for all Throat Diameters as a Function of Magnetic Field Strength

strong applied magnetic field. The onset of the anomalies may thus be associated, in a rough way, with large values of the Hall parameter. If the Hall parameter is large, the current distribution is expected to extend outside the thrustor.[6] It is reasonable to suppose that the existence of currents outside the thrustor favors the occurrence of entrainment processes and arc current - tank interactions.

Thrust Efficiency Dependence on I_{sp}

Thrust efficiency is shown as a function of I_{sp} in Figure 45. The higher points are the efficiency measurements in the 4 to 20 kilogauss range for the smallest throat sizes; the circles give the results of the 1 and 2 kilogauss tests at the smallest throat diameters. The frozen flow curve and some previous measurements[1] for 25 mg/sec mass flow are shown on the same graph for comparison. As discussed above, the high efficiencies at the high specific impulse and magnetic field may be due to arc interaction with the environment.

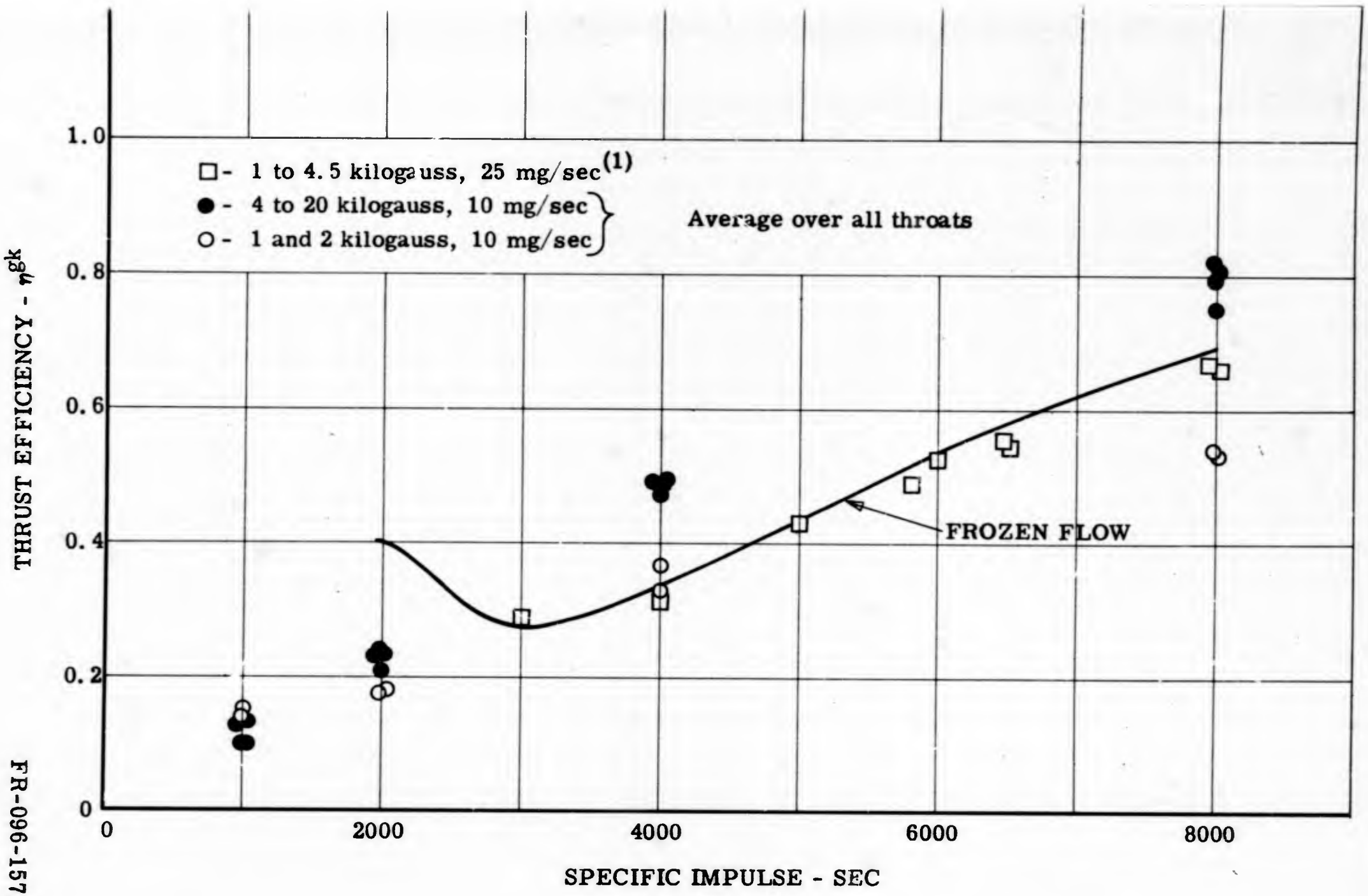

Figure 45. Thrust Efficiency as a Function of Specific Impulse

3.3 Overall Efficiency

The overall efficiency will of course reflect the dependence of η^{eg} and η^{gk} on B and I_{sp} discussed above. Figure 46 shows the overall efficiency as a function of magnetic field strength for the smallest throat used at the specified specific impulse and magnetic field strength. This plot therefore displays the higher efficiency measurements. Figure 47 shows overall efficiency as a function of specific impulse; the data displayed represents the measurements made with the smallest throat size at the specified magnetic field and specific impulse.

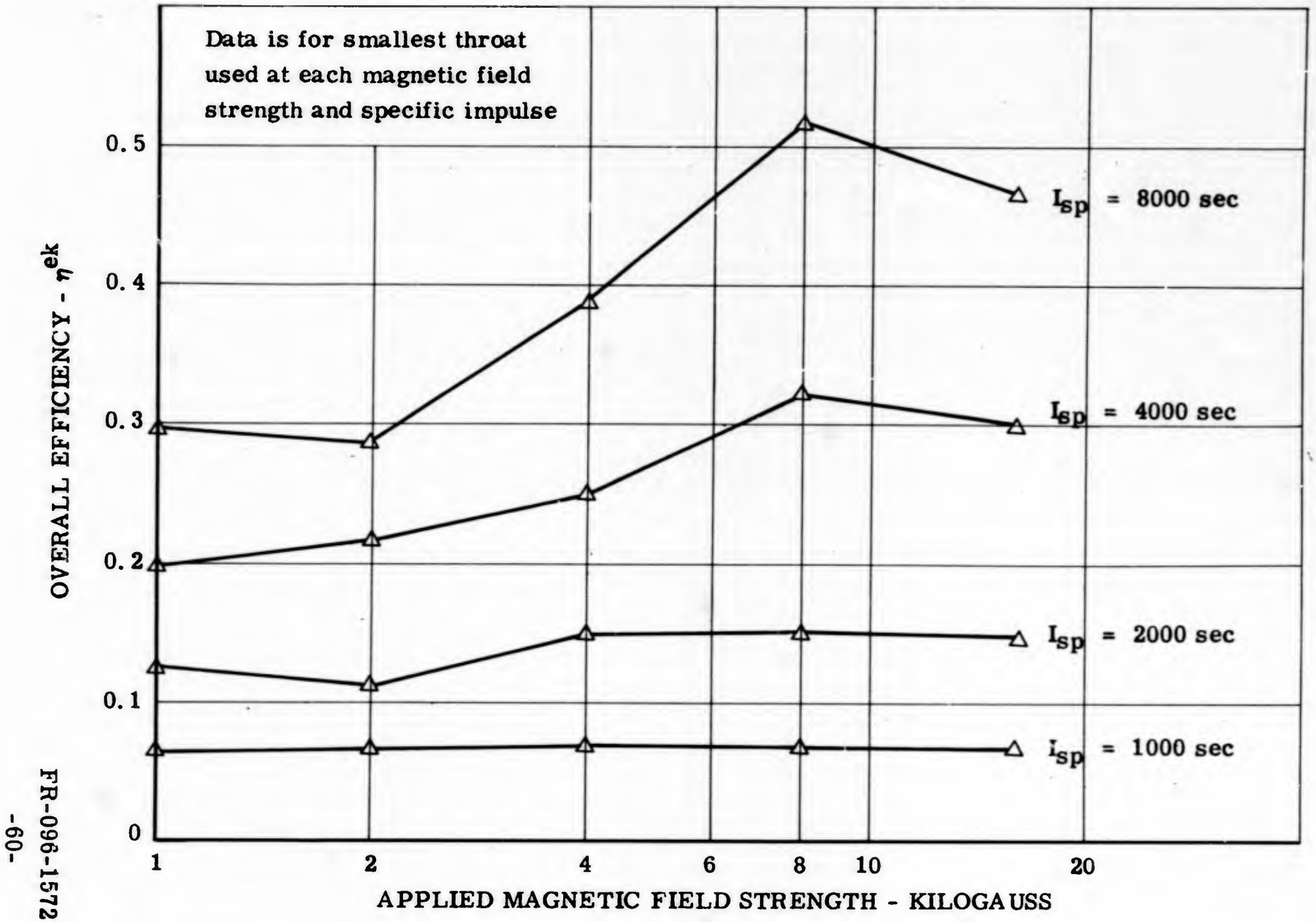

Figure 46. Overall Efficiency as a Function of Magnetic Field Strength

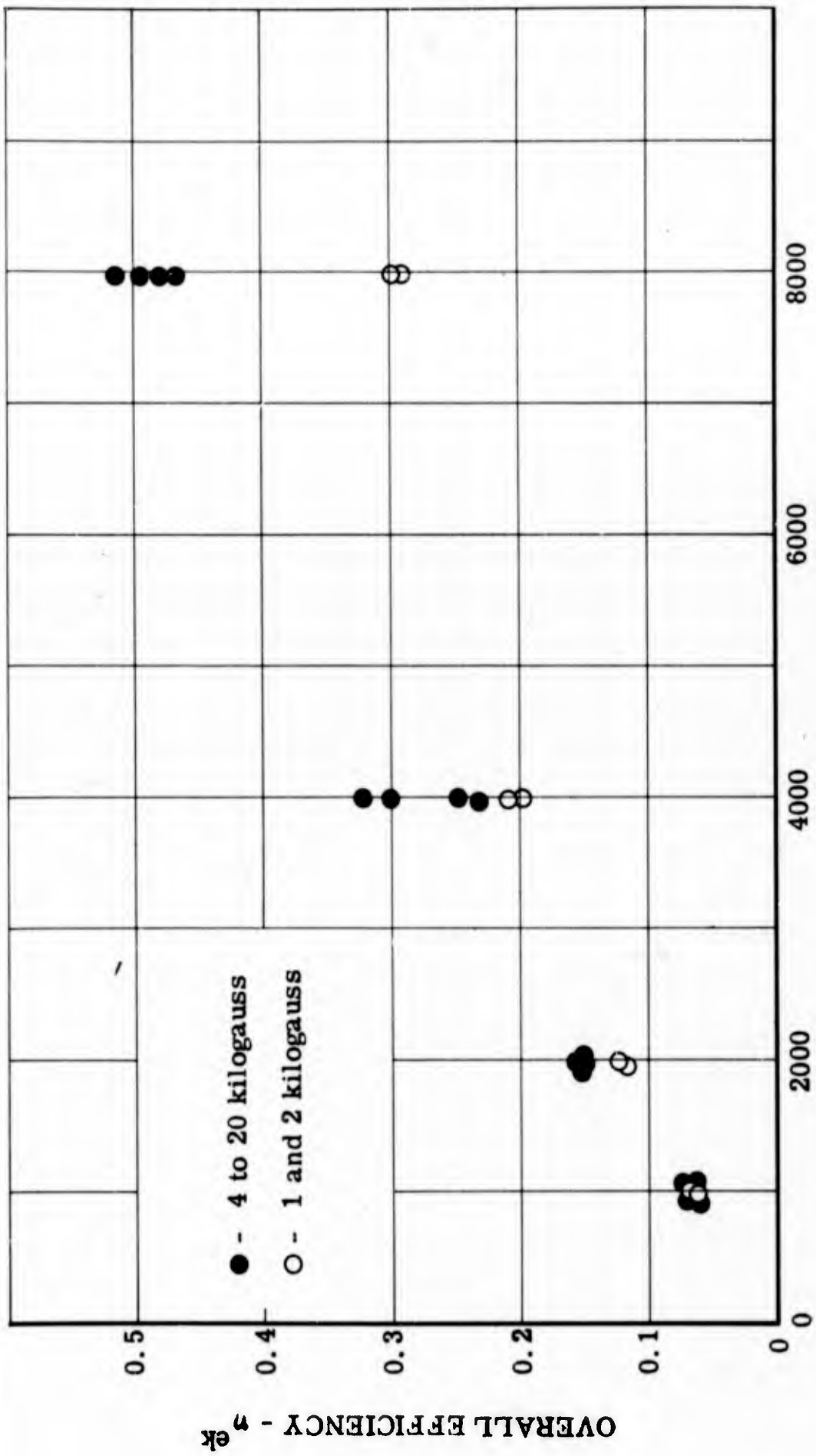

Figure 47. Overall Efficiency as a Function of Specific Impulse for Smallest Throat at Each Magnetic Field Strength and Specific Impulse

3.4 Pressure Effects

The pressure measurements for the 2000 second tests are shown in Figure 48. Let us see how they compare with some one-dimensional flow considerations. Using the continuity equation, the equation of state and the expression for the velocity of sound for a perfect gas, the pressure at the throat can be expressed in the form

$$p^* = \frac{\dot{m}}{A^*}\sqrt{\frac{R\,T^*}{M\,\gamma}}.$$

In this expression A^* and T^* are the throat area and temperature, $\dot{m}$ is the mass flow rate and R, M and γ are the gas constant, molecular weight and ratio of specific heats, respectively. If the temperature in the throat and the ratio of chamber pressure to throat pressure are independent of the throat size then, according to this expression, $p\,A^* = \text{const.}$ A curve $p\,A^* = \text{const.}$ is compared with the pressure measurements in Figure 48. We see, as pointed out in Section 2.2, that there is some disagreement between the pressure measurements and the simple $p\,A^* = \text{const.}$ relation. Inspection of Table 9 shows that there is a definite tendency for thermal efficiency to increase with increasing pressure (or decreasing throat diameter). This pressure dependence and the general problem of determining the plasma and arc parameters on which the thermal efficiency depends is an interesting area for further study, since the present thermal losses are quite large and there is hope that these losses can be reduced significantly.

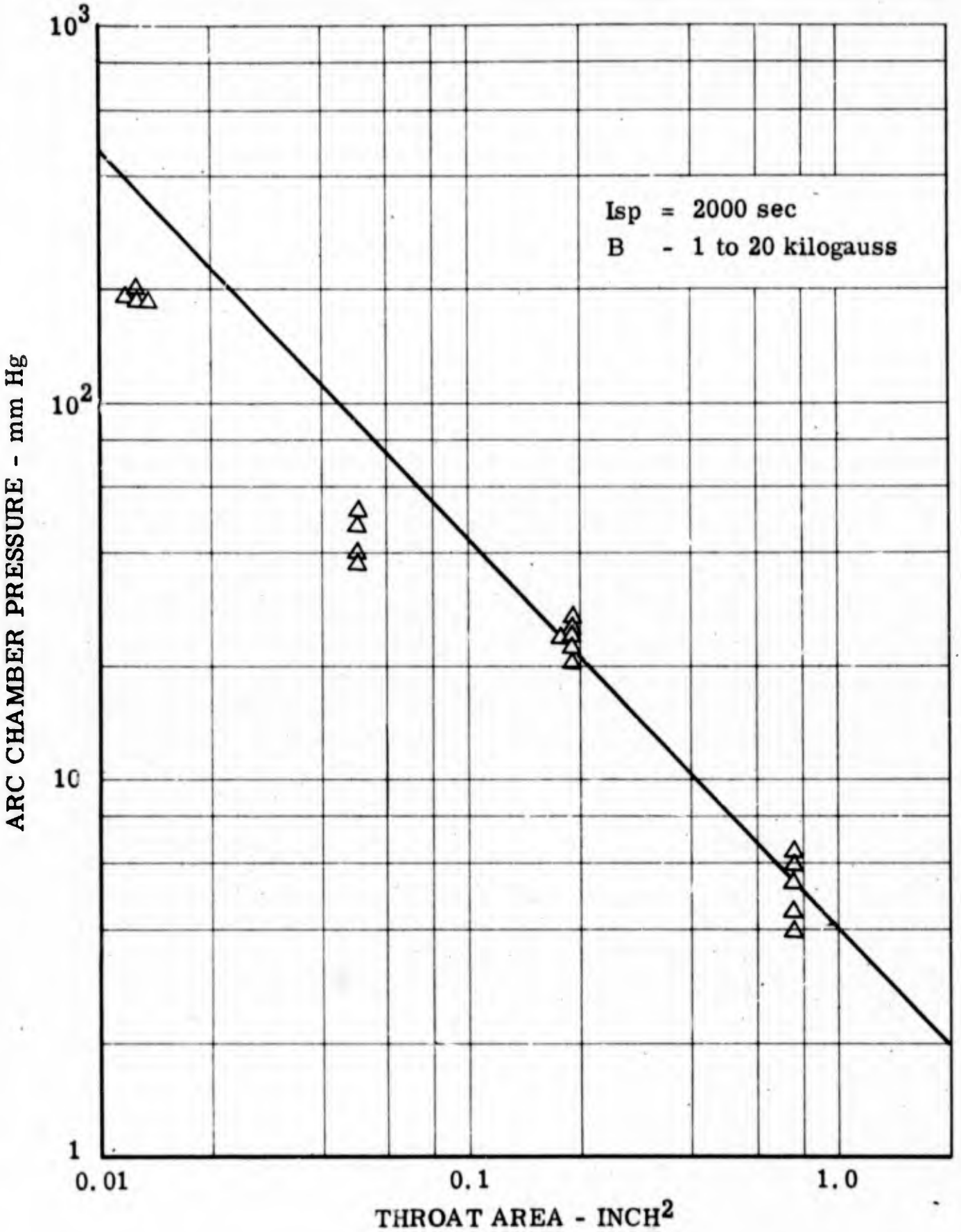

Figure 48. Arc Chamber Pressure as a Function of Throat Area at Constant Specific Impulse at 2000 Seconds

The thrust efficiency is also pressure dependent with the higher efficiencies corresponding to the high pressures. The changes in η^{gk} with pressure are not as large as for the thermal efficiency, but the increases in η^{gk} which are obtained by increasing the pressure are still significant.

3.5 Voltage Characteristics

The variation of voltage with magnetic field strength is shown in Figure 51. The data includes voltage measurements over a 1000 to 8000 second range. The measurements at 16 and 20 kilogauss display irregular behavior and have not been plotted. By inspection of Figure 49 it can be seen that the voltage increases approximately linearly as the magnetic field strength is increased. A linear relation has been observed previously[2, 3] in the 0.5 to 2.0 kilogauss range with H_2 and in the 0.5 to 4.0 kilogauss range[4] with NH_3. The results presented here show that the linear dependence continues to hold up to 8 kilogauss.

It is qualitatively clear that the arc voltage should increase as the applied magnetic field strength is increased. However, in view of the non-linear character of the magnetogasdynamic equations and the complexity of the generalized conduction equation it is surprising that the arc voltage and magnetic field are related linearly. The basic physical processes which establish this linear characteristic do not appear to be very well understood. *

The voltage usually changes very little with specific impulse as is shown in Figure 50. This behavior is a well established property which is characteristic of these low pressure arcs.

---

*See, however, a partial theoretical explanation proposed by Patrick and Schniederman.[3]

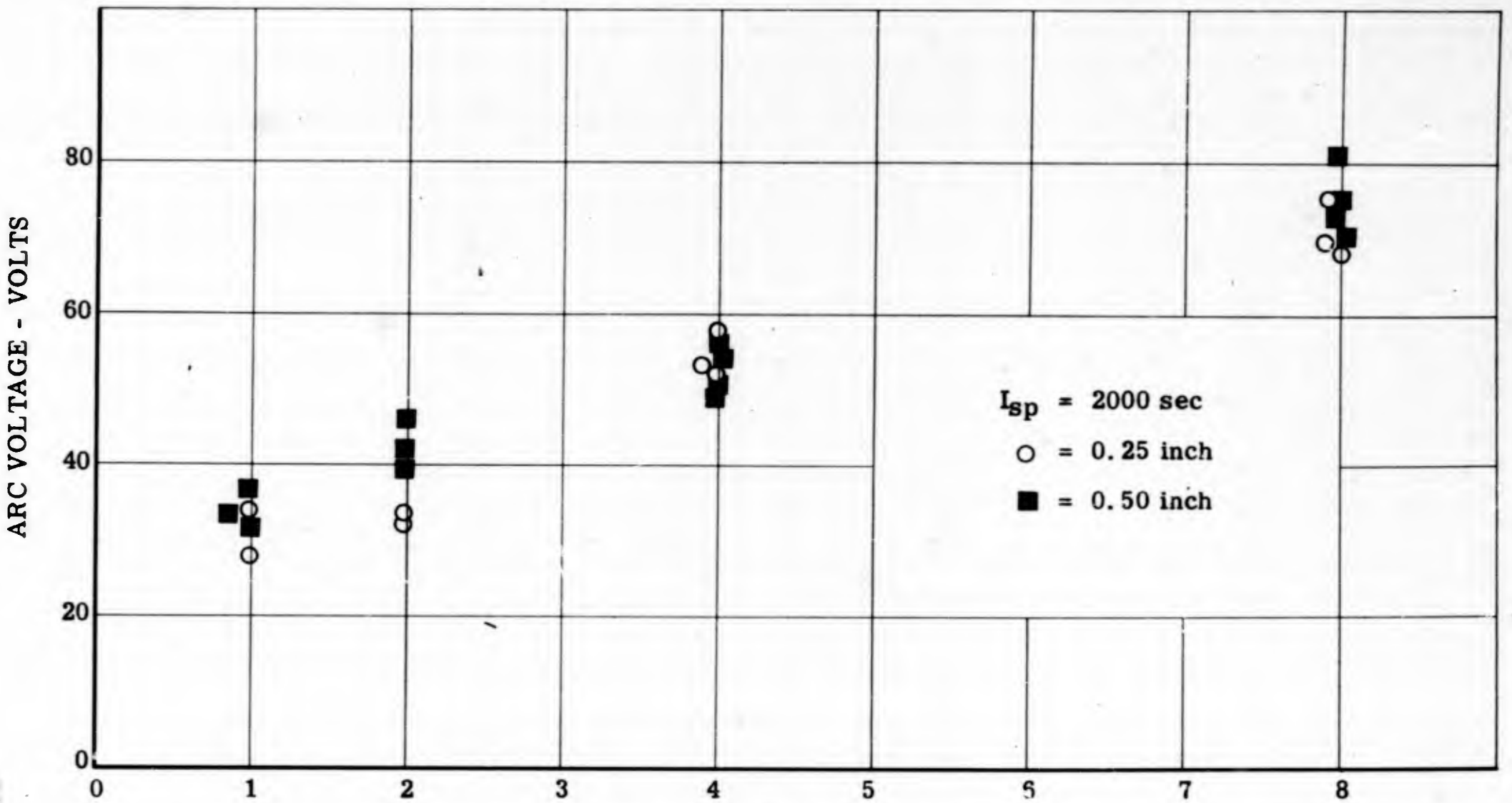

Figure 49. Variation of Voltage With Magnetic Field Strength at 2000 Seconds

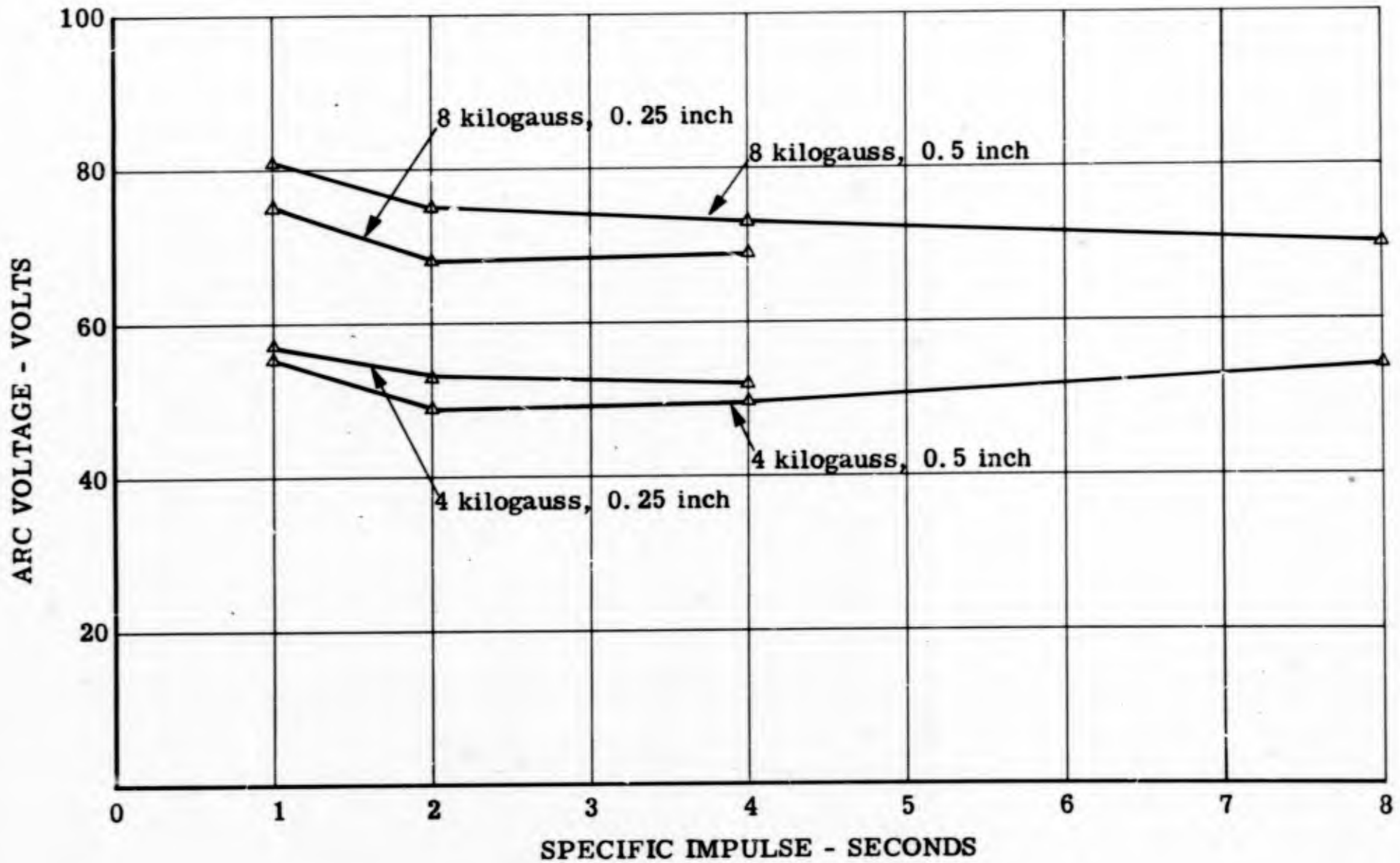

Figure 50. Variation of Arc Voltage With Specific Impulse at Constant Magnetic Field Strength and Throat Diameter

4.0 INTERPRETATION OF RESULTS

4.1 Magnetic Effects

For a current column 1 cm in diameter and a total current of 2500 amps, which are conditions that are easily attained in low pressure arc jets,[7] the magnetic pressure is comparable to the arc chamber pressure. Magnetic forces of the self-induced fields are thus expected to be important, and indeed, magnetic compression, producing pressures considerably larger than the arc chamber pressure, has been observed near the cathode.[2, 7]

When a magnetic field is applied coaxially to the electrode geometry, the arc voltage increases and the current decreases as discussed above. The application of a magnetic field thus tends to diminish the effects of the self-field and, of course, introduce effects associated with the interaction of the arc currents and plasma flow with the applied field. For example, with an applied field of 4000 gauss at 4000 seconds (see Table 9), the arc current is about 500 amps. Magnetic forces associated with this current are considerably smaller than those corresponding to an applied field of 4000 gauss. In the following discussion we shall consider only the effects of the applied field and the arc jet.

Initially it was hoped that by use of a coaxial magnetic field the thermal and thrust efficiencies could be increased significantly.[4] This has proved not to be the case for the thermal efficiency, as previous tests in the 0.5 to 2.0 kilogauss range,[1, 2] and the results presented here for 1 to 20 kilogauss fields have shown. The effect of the applied field on the thrust

efficiency is still not known with certainty because of the problem of spurious interactions, however there is considerable evidence that the applied field acts mainly as a nozzle while imparting angular momentum to the flow.

First let us review some basic aspects of the arc jet flow in a strong field. By looking at the arc jet it appears that the plasma flow follows the magnetic field lines for, say, $B \geq 2000$ gauss (see Figure 21). As the magnetic field is increased the luminous region of the jet undergoes changes described in Section 2.3, which imply that the diffusion perpendicular to the field lines is very small. The diffusion velocity perpendicular to B is given by[8]

$$V_{D,\perp} = \frac{\eta_\perp p}{B^2 r}$$

while the axial velocity of the plasma may be taken as the sound speed

$$V_z = \sqrt{\frac{\gamma R T}{M}},$$

where $\eta_\perp$ is the resistivity[8] of a fully ionized hydrogen plasma, p is the kinetic pressure and r is a significant radial dimension of the flow. The equation for V_z is the expression for the velocity of sound in a perfect hydrogen gas. With $r = 1/2$ cm, $B \geq 2000$ gauss, $T > 10,000°K$, then $V_{D\perp}/V_z << 1$. Under these conditions it is to be expected that the plasma flow will follow the magnetic field lines. Consideration of the magnetogasdynamic equations shows more explicitly that the applied field acts as a nozzle.[6] That is, by inspection of the momentum equation one

can see that the Lorentz forces due to the induced azimuthal currents just balance the centrifugal forces and pressure gradients perpendicular to the magnetic field lines thereby confining the flow and producing the same effect as a metal nozzle. The applied field is also the cause of another effect which we shall discuss below.

Torque on the Flow

It is well-known that the interaction of the arc currents with the applied magnetic field produces a rotational motion of the plasma. This motion has been detected by visual observation of the jet and has also been inferred from swirling erosion and deformation patterns observed at the electrode surfaces.

Let us consider this rotational motion caused by the applied axisymmetric magnetic field. The torque acting on the plasma is given by

$$L = \int r\, j_\perp\, B\, dv \qquad (6)$$

where dv is an infinitesimal volume element and $j_\perp B = (\vec{j} \times \vec{B})_\theta$ is the component of the Lorentz force per unit volume acting in the θ-direction, which causes the rotation of the plasma. The integration of the torque density $r\, j_\perp\, B$ over the volume of plasma where $j_\perp$ is nonvanishing gives the total torque on the flow. The integral in (6) may be written in the form

$$\frac{1}{2\pi} \iint d\,I\, d\,\Phi$$

where

$$dI = 2\pi j_{\perp} r\, ds$$

is the current crossing an infinitesimal cylindrical surface of radius r and length ds tangent to the magnetic field lines, and

$$d\Phi = B\, dA$$

is the flux through an annular area dA perpendicular to the field lines. Carrying out the integration over the cylindrical surfaces defined by the magnetic field lines (surfaces of constant Φ) yields

$$L = \frac{1}{2\pi}\int I(\Phi)\, d\Phi \qquad (7)$$

where the limits of integration will depend on the particular current distribution. $I(\Phi)$ is the current flowing through a surface of constant Φ. The integral in (7) can be evaluated for certain idealized current distributions as we show below.

Current Flow Confined to the Throat

Consider an axisymmetric current distribution of the type illustrated in Figure 51.

Suppose the current density at the cathode is a δ-function distribution at the radius $r_{c'}$, i.e.,

$$j = \frac{I\,\delta(r - r_{c'})}{2\pi r_{c'}}$$

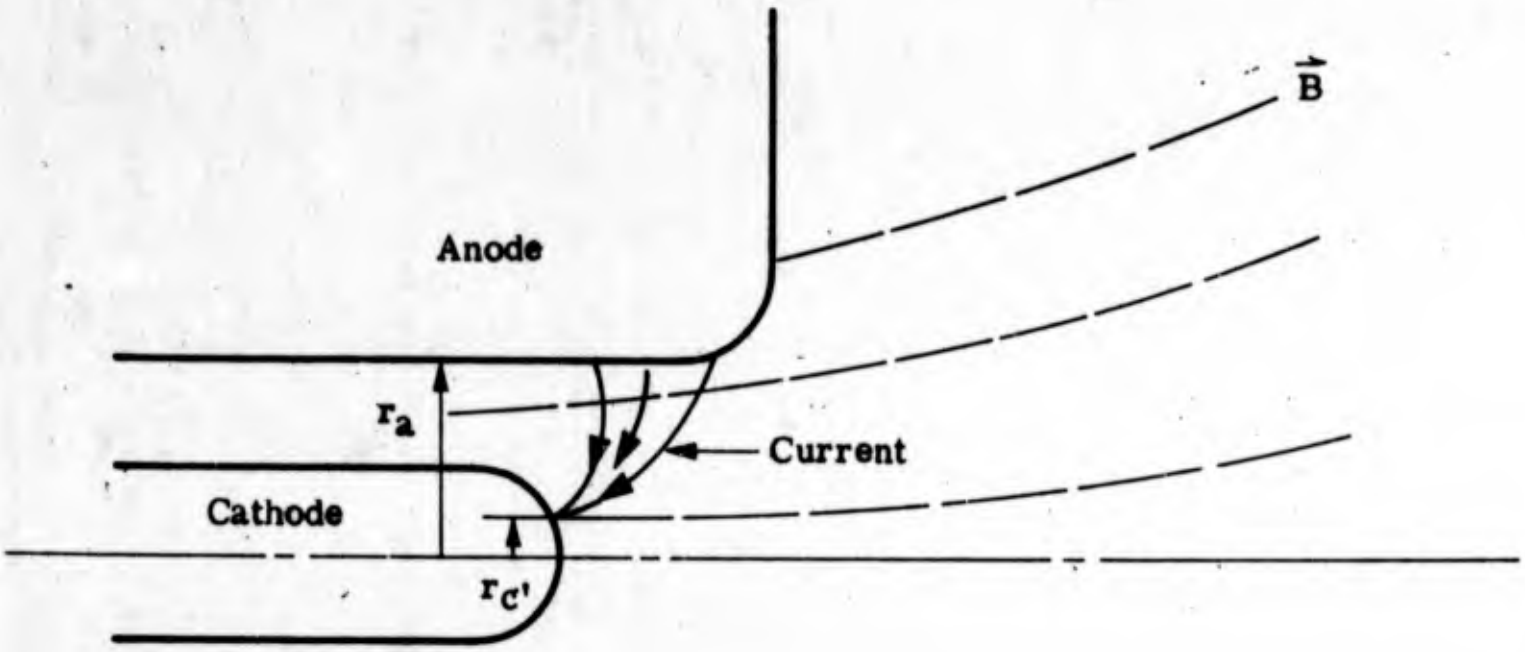

Figure 51. Current in the Throat and a δ-Function Distribution at the Cathode

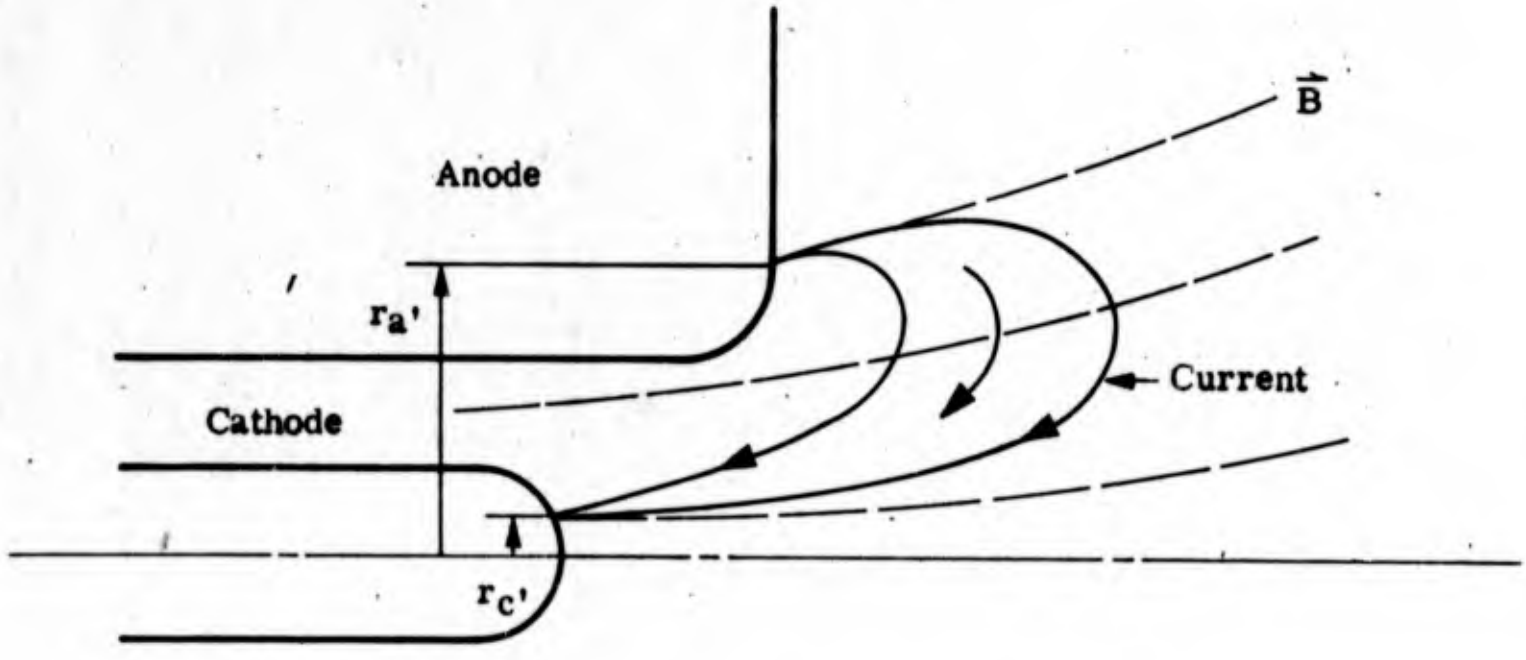

Figure 52. Current Outside the Throat and δ-Function Distributions at Anode and Cathode

where I is the total arc current and $\delta (r - r_{c'})$ is the Dirac delta function. The current density is arbitrary at the anode except that currents may not extend outside the throat. For such a current distribution the integration can be carried out with the result

$$L = \frac{I \Phi_{c'a}}{2 \pi} \tag{8}$$

where $\Phi_{c'a}$ is the flux in the annular area bounded by circles of radii r_a and $r_{c'}$:

$$\Phi_{c'a} = 2 \pi \int_{r_{c'}}^{r_a} B (r) \, r \, d r \, .$$

If $r_c \rightarrow 0$, then $\Phi_{c'a}$ becomes the total flux in the throat and equation (8) gives the torque for the case of a current emanating from the tip of the cathode. If this assumed current distribution is representative of the actual condition in the flow, the torque will be given by (8). If the radius $r_{c'}$ of the cathode current is known, then one can calculate the torque accurately since the magnetic field distribution B (r) can be determined. -

δ-Function Distribution at Anode and Cathode

Consider the current distribution illustrated in Figure 52. The distribution in regions away from the electrode surfaces is completely arbitrary. The torque on the plasma obtained by integration of (7) is then

$$L = \frac{I \Phi_{c'a'}}{2 \pi} \tag{9}$$

where $r_{a'}$ is the radial position of the circular anode current distribution and may be located anywhere inside or outside the throat. The flux is given by

$$\Phi_{c'a'} = 2\pi \int_{r_{c'}}^{r_{a'}} B(r)\, r\, dr .$$

If the radii of the attachment of the cathode and anode current distribution is known, then the flux, given by the above integral can be evaluated and the total torque on the flow calculated with the aid of (9).

It is also interesting to consider the general case of arbitrary anode and cathode current distribution. We then have the torque

$$L = \frac{I\,\Phi_{ca}}{2\pi} + \frac{1}{2\pi}\int_{0}^{\Phi_c} I(\Phi)\, d\Phi + \frac{1}{2\pi}\int_{\Phi_a}^{\Phi_{a'}} I(\Phi)\, d\Phi .$$

Since the integrals are not negative quantities it follows that

$$L \geq \frac{I\,\Phi_{ca}}{2\pi} . \qquad (10)$$

Φ_{ca} is the flux in the minimum channel area $\pi(r_a^2 - r_c^2)$ and $\Phi_{c'}$, $\Phi_{a'}$ and $\Phi_{a'}$, are the fluxes through the areas bounded by circles of radii r_c, r_a and $r_{a'}$. The inequality (10) is of very general validity as it holds regardless of the details of the electrode geometry and current distribution.

Furthermore, (10) is expressed in terms of quantities which are measurable. Let us state this result more precisely.

Suppose in a coaxial electrode geometry the flow is time independent, axisymmetric, electrically neutral, has a scalar pressure, and the inviscid magnetogasdynamic description of the flow is valid. Then the magnitude of the angular momentum imparted to the flow by the interaction of the arc currents with an applied magnetic field (and felt as a reaction torque on the thrustor) satisfies the inequality (10).

This inequality can be used to demonstrate that for very strong applied magnetic fields the current distribution must be at least partly outside the throat. This is shown as follows.

The flux of angular momentum through a surface through which the entire flow passes and which is downstream of the current distribution is equal to the total torque on the flow, and is given by

$$L = \int r v_\theta \, d\dot{m} \tag{11}$$

where $d\dot{m}$ is an infinitesimal element of the mass flow rate. The flow will have the least energy for the same angular momentum if the flow is concentrated at the largest radius of the flow. If the current distribution is confined entirely to the throat this radius may be taken to be the anode radius r_a. Expressing the angular momentum flux as

$$\int r\, v_\theta \, d\dot{m} = r_a \, \bar{v}_\theta \, \dot{m} \tag{12}$$

defines an azimuthal velocity $\bar{v}_\theta$. Calculating the rotational power in the flow with $\bar{v}_\theta$ will give a value less than the actual value. Hence, from the inequality (10) and equations (11) and (12) follows

$$\bar{v}_\theta \geq \frac{I \Phi_{ca}}{2 \pi r_a \dot{m}}$$

and consequently

$$P_\theta > 1/2 \, \dot{m} \, \bar{v}_\theta^2 \geq \frac{1}{8 \pi^2 \dot{m}} \left(\frac{I \Phi_{ca}}{r_a} \right)^2 \tag{13}$$

where P_θ is the rotational power in the flow.

Consider the following experimental results. For $\dot{m} = 10$ mg/sec, throat diameter 1.0 inch, cathode diameter 0.625 inch, $B = 4000$ gauss and $I = 500$ amps, the power in the gas was 17.5 kw at a specific impulse of 4000 seconds. Using these numbers in (13) gives

$$P_\theta = 31 > 17.5 \text{ kw}$$

which is in disagreement with the principle of the conservation of energy. This implies that it is not possible, under these conditions, to have the current distribution entirely in the throat. If the currents cross the magnetic field outside the thrustor, the radial dimension in the denominator of equation (13) corresponding to the physical situation is much larger than the inner anode radius and thereby one calculates less rotational power in the flow and achieves compatibility with the conservation of energy.

4.2 Thermal Efficiency

The experiments conducted here and also at Avco RAD[2] have shown that as the specific impulse increases the thermal efficiency becomes constant, i.e., the power loss to the electrodes is proportional to the total power in the gas. This suggested that a good fit of the data over the entire range of measurements could be obtained by assuming an electrode power loss of the form

$$P_a = \lambda \dot{m} V_{ex} + \varkappa \dot{m} h \qquad (14)$$

where $\varkappa$ and λ are arbitrary constants. In equation (14), $\dot{m}$ is the mass flow, h is the specific enthalpy including ionization and dissociation potential energy, and V_{ex} is a constant energy per unit mass associated with an average excitation energy level of atomic hydrogen.

The term which is linear in the specific enthalpy should be associated with convective and conductive heat transfer to the electrodes. The term $\lambda \dot{m} V_{ex}$ is identified with the line radiation absorbed by the electrodes. The radiation loss is taken in this form to express the idea that each heavy particle, in passing through the discharge, undergoes a certain number of excitation collisions and a subsequent transition to the ground state with the emission of a quantum of radiation, which we are assuming is absorbed by the electrodes. The energy per unit mass of the average excitation level is denoted by V_{ex} and the average number of excitation collisions per particle is given by λ. Since we lack a detailed knowledge of the excitation and radiation processes, for simplicity the radiation term is taken to be

constant. Bremsstrahlung is negligibly small for electron temperatures and densities thought to exist in these low pressure arc jets and thus need not be considered.

Using (14) the thermal efficiency can be written in the form

$$\eta^{eg} = \frac{1}{1 + \varkappa + \frac{\lambda V_{ex}}{h}} . \qquad (15)$$

The thermal efficiency calculated from equation (15) is shown in Figure 53. The parameters λ and $\varkappa$ have been chosen to obtain a fit of the data, which is seen to be good. It is clear from equation (15) that the magnitude of $\varkappa$ determines the losses at the higher specific impulses.

The power loss of the form of (14) would not seem reasonable if conduction were a dominant heat transfer process. If this were the case, one would expect the coefficient $\varkappa$ to be strongly dependent on temperature and magnetic field strength. The good fit might be interpreted as an indication that the heat transfer is primarily due to the convection by electrons. This is merely a correlation of the data and may be considered a first step in understanding the thermal losses. More important is the investigation of the physical processes which determine the magnitude of the thermal loss. With the analytical form for the electrode losses given above this would mean the investigation of the physical factors which determine the magnitude of the arbitrary parameters $\varkappa$ and λV_{ex}.

We shall now discuss a highly idealized and incomplete analytical model for the power loss to the electrodes, which also has the nature of a fit, but

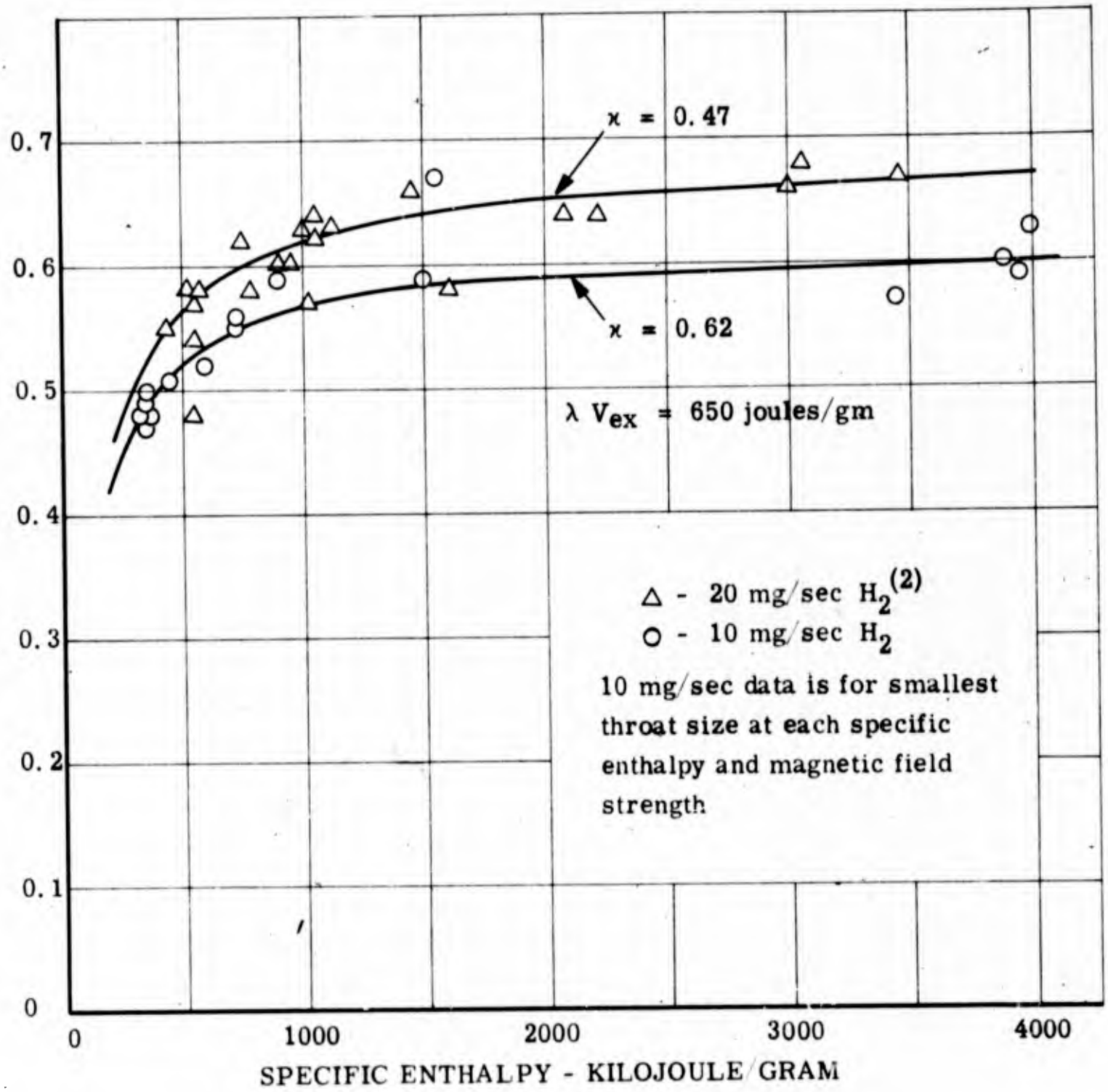

Figure 53. Two Parameter Fit of Thermal Efficiency Measurements Based on Assumption That Electrode Power Loss is Proportional to the Specific Enthalpy Plus a Constant

proceeds a little further towards a physical model of the electrode losses. The discussion will apply to arc operation in the high range of specific impulse with a strong applied magnetic field. More precisely, it will be assumed that the mass flow is "parallel" to the magnetic field lines and that the main current path extends down the axis of the flow and then, somewhere well downstream from the electrode surfaces, turns radially, crosses the field lines and then returns to the anode parallel to the field lines. This current distribution is consistent with an analysis by Jahn[6] of arc current distributions for conditions where the Hall parameter is much greater than unity near the electrode surfaces.

The arc is considered here to be composed of three distinct voltage drops, although in the actual arc they must merge continuously into one another. These voltage drops are associated with the axial flow of currents at the cathode; the "radial" current flow, and the current flow parallel to the magnetic field lines at the anode. The anode voltage drop is associated with the entire length of the anode current distribution from the anode to where the radial current flow develops and not necessarily just to a narrow region near the anode. Applying the energy balance equation to the annular region illustrated in Figure 54 yields the anode power loss in the form

$$P_a = I V_a - \int \vec{q} \cdot \vec{dA} \qquad (16)$$

where V_a is the anode voltage drop, I is the total electrical current, and thus $I V_a$ is the total electrical power input to the anode current

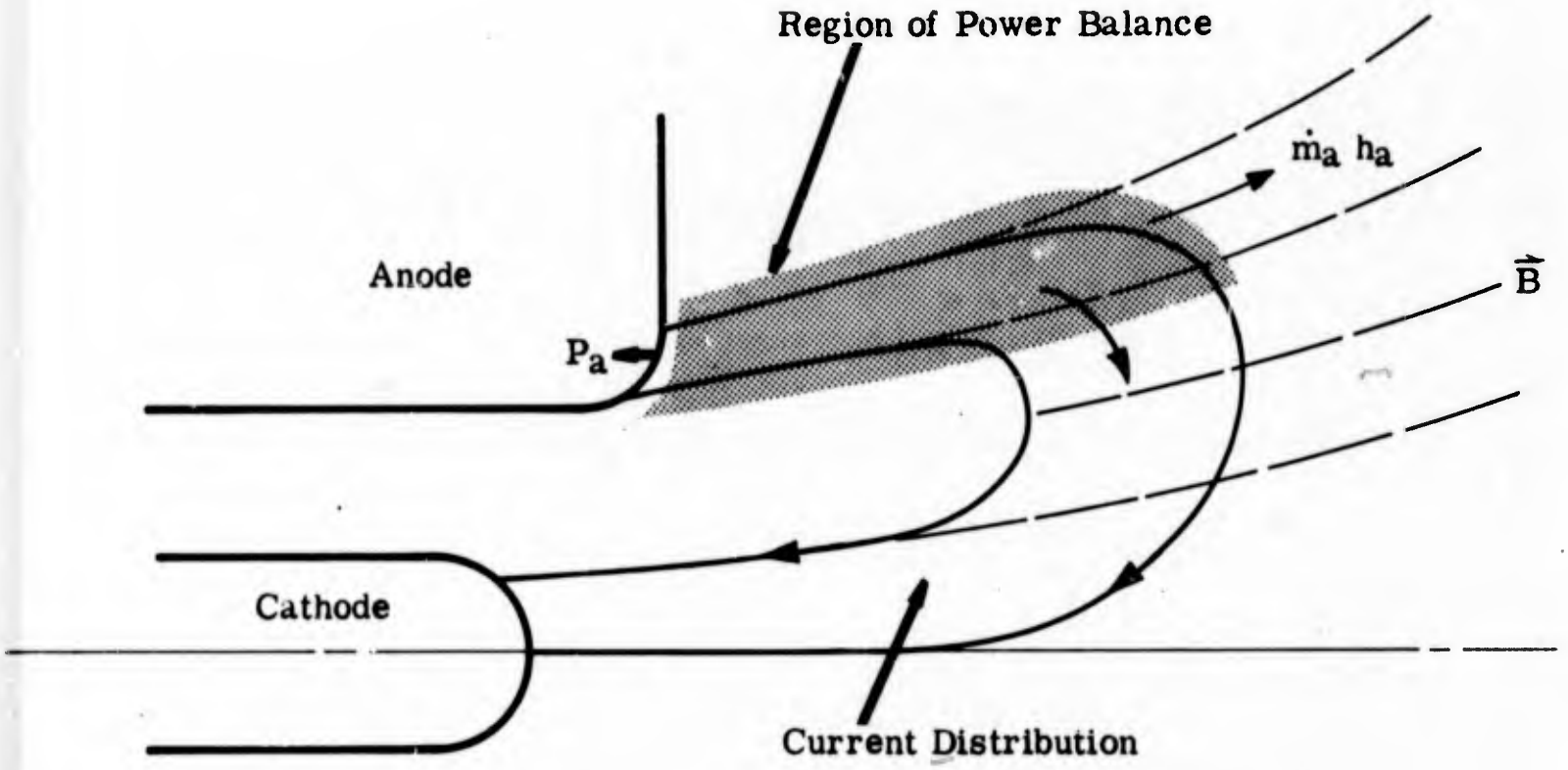

Figure 54. Region of Power Balance and Current Distribution for Strong Magnetic Field, High I_{sp} Conditions

region in the periphery of the flow. This region of the flow is often called the anode jet. The integral in (16) represents the total power transfer through the surface, excluding the anode surface, which bounds the annular region of the anode current flow. Radiation will be neglected since it should be small for these low density flows. The convective transfer of energy by electrons into the anode region is probably small for the following reasons. The electrons must undergo considerable cooling by expansion as the radial current flow develops and, in addition, even though there may be a large electrical power input into the region of radial current flow it is likely that this power will go mainly into rotational motion of the mass flow, as discussed in Section 4.1, and not into electron temperature. Enthalpy flux in the radial direction is excluded by our assumption of no mass diffusion across the magnetic field lines, which leaves the total enthalpy flux (including potential energy of dissociation and ionization) along the field lines as the major contribution to the integral in equation (16). According to these arguments the anode power loss can be approximated by

$$P_a = I V_a - \int_{\dot{m}_a} h \, d\dot{m} \qquad (17)$$

where the integration is over the mass flow leaving the region of electrical power input in the peripheral region of the jet.

The sum of the power loss to the cathode and the loss to the arc chamber are usually small compared with the anode loss and will be neglected

henceforth. Then, with (17), the thermal efficiency may be expressed in the form

$$\eta^{eg} = \frac{1 - V_a/V}{1 - \dot{m}_a\, h_a/\dot{m}\, h} \tag{18}$$

where we have used

$$\int_{\dot{m}} h\, d\dot{m} = \eta^{eg}\, P$$

and the notation

$$\dot{m}_a\, h_a = \int_{\dot{m}_a} h\, d\dot{m} \quad , \quad \dot{m}\, h = \int_{\dot{m}} h\, d\dot{m}$$

for the power leaving the anode region and the total power in the jet respectively.

As the power to the arc is increased at a fixed magnetic field strength, the arc voltage and thermal efficiency stay nearly constant. If the ratio of the power in the peripheral part of the flow to the total power in the flow remains constant, this implies that the anode voltage V_a is approximately constant. This aspect of the thermal losses has been noted previously.[2, 4, 5] That is, it has been observed that thermal efficiency measurements could be correlated by the assumption that the thermal power loss is associated with a constant anode voltage drop. It is clear that here, and in the

references cited above, the power loss is attributed primarily to a convective transfer process.

When the applied magnetic field strength is increased the voltage increases linearly with B and the thermal efficiency remains approximately constant. If the ratio of enthalpy flux in the periphery of the flow to total enthalpy flux remains the same, then, according to (18), this implies that the anode voltage V_a also increases linearly to maintain V_a/V constant. Thus, according to this model for the thermal losses in the high range of specific impulse, the ratio of the voltage associated with the current flow in the peripheral region of the arc to the total voltage is approximately independent of power and magnetic field strength for fixed mass flow rate and electrode geometry.

It is of course of practical interest to establish the factors which determine the voltage ratio V_a/V and to invent ways of decreasing it.

The voltage drop V_a associated with the anode region of the current flow can be related to the parameter $\varkappa$ appearing in equation (14). We have, for $\lambda V_e/h << 1$,

$$\eta^{eg} \approx \frac{1}{1+\varkappa}$$

which with (18) gives

$$\frac{V_a}{V} = \frac{\varkappa + \dot{m}_a h_a/\dot{m} h}{\varkappa + 1} . \qquad (19)$$

We see that in this model for the power loss for the strong field, high I_{sp} conditions, the parameter $\varkappa$ is associated with the anode potential and the ratio of the enthalpy flux in the peripheral part of the flow (or anode jet) to the total enthalpy flux.

4.3 Thrust Efficiency

It is now well established that at low mass flow rates the thrust efficiency can exceed the frozen flow efficiency and in fact be larger than 100 percent. Experiments at Avco RAD[2] have shown that ingestion and acceleration of ambient gas can cause these high efficiencies. There is also a possibility that under some conditions electrode vaporization [9] and perhaps interaction of the arc currents with the tank can also contribute to erroneous results. If electrode vaporization takes place one can weigh the electrodes before and after a test to correct for this contribution to the flow. Interactions of the arc with the tank can probably be eliminated by use of a suitably designed test tank.[1, 10] However, the solution to the entrainment problem is presently not evident. Even if one were able to determine the entrained mass and make appropriate corrections to the efficiency calculations, this would not be a completely satisfactory solution. For there is then no assurance that the performance would be the same, or even that the arc would work at all, in the hard vacuum of free space. A more satisfactory solution to this problem would be to reduce entrainment effects to negligible amounts in a terrestrial test environment.

The anomalously high efficiencies occur at very low mass flows. Let us consider some data which illustrates the strong dependence of thrust efficiency on mass flow rate. Figure 55 shows this dependence for various values of specific impulse. For clarity we have connected points of equal specific impulse with straight lines. The points at 10 mg/sec are averages of the data presented in Table 9. The 3, 5, 12.5 and 50 mg/sec points are

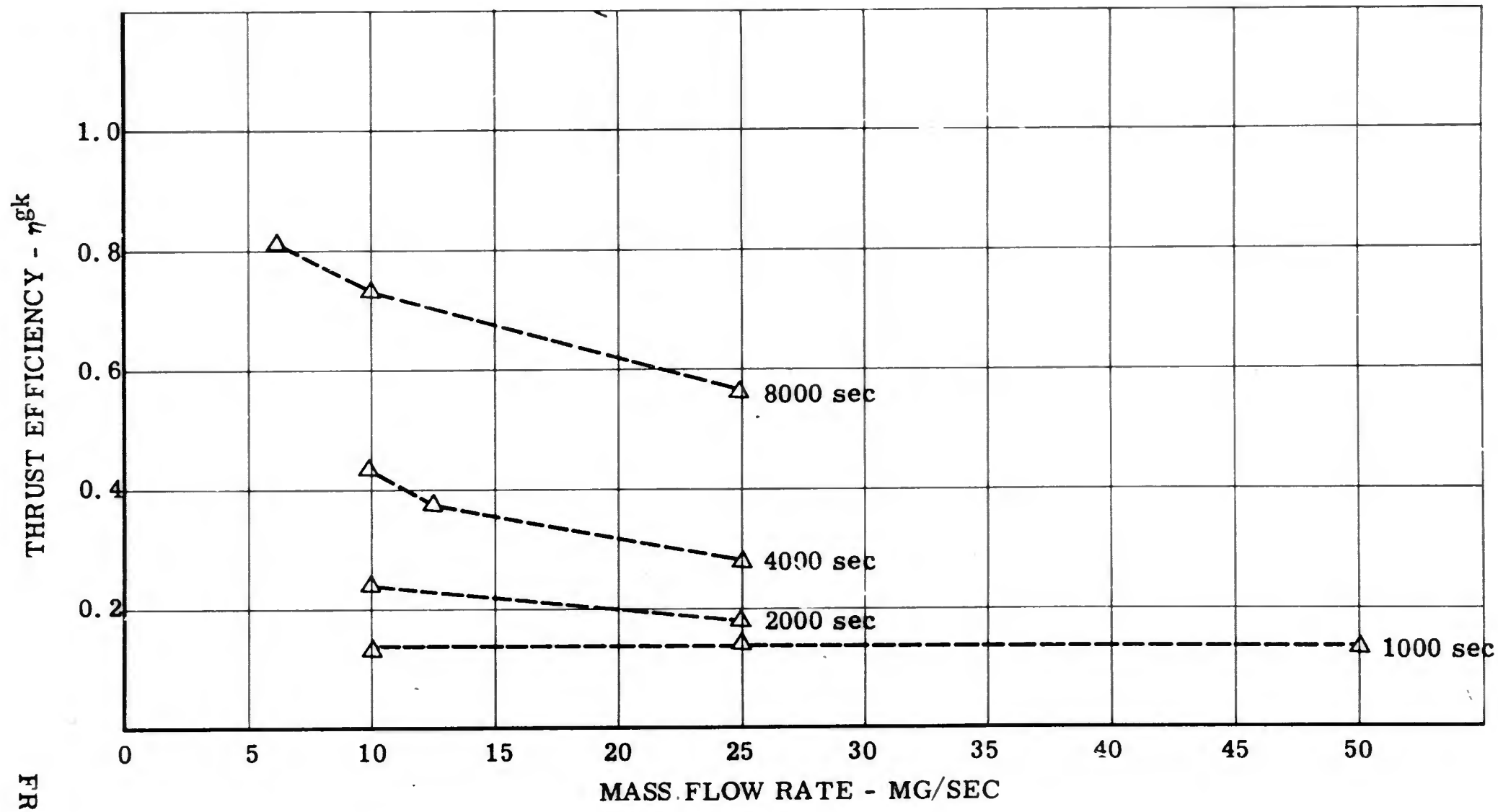

Figure 55. Variation of Thrust Efficiency With Mass Flow Rate

previous test results reported in Reference 1. Test results in the same range of mass flows reported by Avco RAD[2] and EOS[5] are not considered with the data shown in Figure 55 because of important differences in the electrode configurations.

The thrust efficiency at 1000 seconds is seen to be independent of mass flow rate. This is roughly what is expected for a thrustor with a constant expansion efficiency under conditions where ambient pressures are low enough so that changes in ambient pressure should not affect the thrust appreciably. At specific impulses greater than 2000 seconds the thrust efficiency increases rapidly as the mass flow decreases. This increase is much too large to be explained on the basis of decreasing tank pressures or increased expansion efficiency.

It appears that at 25 mg/sec flow the expected dissociation and ionization losses are occurring, while at the low mass flows effects exist which increase the apparent efficiency significantly. In the range of low particle density and high temperature where these anomalously high efficiencies occur the Hall parameter is large, which produces conditions that cause the currents to flow outside the thrustor. If the currents and consequently a region of energy addition exist outside the thrustor it makes the assumption of entrainment as the cause of the increase in thrust efficiency plausible. The initial approach[2, 11] to eliminate entrainment has been to reduce the ambient tank pressure to very low values (less than 10^{-4} mm Hg) and thereby decrease the diffusion of ambient gas into the heating and accelerating regions of the arc. This approach may not

eliminate the problem. The reason appears to be that the surface area of the current distribution outside the thrustor increases as the tank pressure is reduced so as to continue to ingest and accelerate appreciable amounts of ambient gas, even though the ambient particle density is greatly reduced.

In view of these considerations, it may be useful to examine an alternative aspect of the problem. That is, it may be possible, with suitable electrode configurations and magnetic field distributions, to produce arcs which are not so susceptible to entrainment or other spurious effects, and without a sacrifice in efficiency. For example, with a large throat length to diameter ratio and moderate magnetic field strengths, entrainment effects may not be so severe. For this reason, we are interested in the possibility that the rather sudden jump in thrust efficiency displayed in Figure 46, which occurs in the transition to a range of large Hall parameter, is showing the onset of entrainment. This unwanted interaction may not be operative for conditions corresponding to the lower efficiencies and smaller values of Hall parameter.

5.0 DISCUSSION OF FUTURE WORK

5.1 Future Development of Testing Facilities

During the next period some parts of the experimental facilities will be modified and improved to fulfill needs which became apparent during this study period. The principal modifications will be made in the thrust stand, in the vacuum tank and in the electrodes. Nonmagnetic materials will be used throughout, and surfaces will be protected with a layer of insulating material exhibiting a very low vapor pressure. The vacuum tank and the thrust stand will be separated from the ground with low capacity insulators. Any connection to the thrust stand and plasma generator will be separated from the ground with insulation transformers or other similar systems. All the connections to the plasma generator and its auxiliary circuits will be similarly insulated from the ground. All connections to the thrustor and its accessories will be protected in a neutral metal envelope to avoid any secondary discharge in the highly ionized atmosphere surrounding it. Only a very small frontal area of the plasma generator will be connected to the anode and will be the only point of return of currents circulating outside the arc chamber. A continuously variable, coaxial, magnetic field capable of reaching values of over 25 kilogauss will be also enclosed in the neutral metal envelope and will be capable of continuous operation at the maximum values without influencing the thrust readings. To improve the thrust readings and at the same time make them more quickly, a new magnetic dampener of high power will be used to minimize the oscillations of the thrust beam and to reach a stop position

in the shortest possible time. Improvements in the water-cooling and in the stability of the zero reading will also be applied together with systems to keep them under continuous control. Special electrodes covering all the geometries to be tested will be constructed with improved cooling and fast interchange characteristics. The main vacuum system cannot be improved greatly for economic reasons but various modifications will be introduced to obtain the best pumping rate and the minimum absolute pressure. At the lower mass flows, working pressures near 10^{-3} mm are anticipated. For the tests without propellant throughput the small diffusion pump facility will be reactivated and improved to work possibly around 10^{-4} mm. The instrument recording system will be improved to meet new exigencies of accuracy and speed. The use of color photography to record the plasma jet details will be extended.

5.2 Future Experimental Work

During the next work period the experiments will be extended to a broader range of conditions, and some experiments will be repeated. The planned measurements using the twenty geometries will be continued and possibly finished. Initially these measurements will be conducted in the presently used testing facility, with the use of an insulating secondary chamber inside the main metal chamber as the only modification. Some of the measurements reported here will be repeated but with the use of the insulating chamber; the data with and without the insulation will be compared. As soon as the new internally insulated, nonmagnetic testing facility will be ready, a third series of measurements will be conducted and extended successively to all the geometries planned. During these tests the regular simultaneous recordings of arc pictures and performance data will be continued. Finally, a complete tabulation and cross-reference of all the data available will be prepared.

During the next experimental period (after the termination of the comparison of the first data) a special effort will be dedicated to the development of a thrustor design capable of minimizing the anomalous influences of the arc environment with the objective of obtaining predictable operation in the high vacuum condition of deep space. The use of secondary electrodes and of special geometries, initiated during this period (see Section 2.3), will be investigated in more detail. While hydrogen propellant will still be used primarily, other propellants and electrode metal vapors will be used to a limited extent.

5.3 Future Theoretical Work

The thermal efficiency characteristics of the arc jet with hydrogen propellant are becoming established through experimental investigations. We have obtained a two-parameter fit of this data over a wide range of specific impulse and magnetic field strengths, but there is still very little understanding of the physical factors which determine this loss. Some progress has been made here in the development of an analytical model for the heat transfer, and it appears useful to continue with this analysis.

The electromagnetic rotation of the plasma has been studied here and expressions for the torque on the flow have been derived which have not been obtained previously. In the case of strong fields, the rotational motion appears to be one of the important aspects of the problem of establishing the nature of the energy transfer processes. That is, the transfer of rotational power to the flow appears to proceed through electromagnetic interactions which are not primarily dissipative. Although this aspect of an arc jet flow in a strong field is widely recognized, it is one where quantitative theoretical analysis is needed.

The general problem of determining what parts of the arc voltage drop are due to ohmic dissipation and the part due to essentially nondissipative processes (if these can be uncoupled) is an interesting area for future study. This problem appears to have strong bearing on both the anode losses and the question of the extent to which the energy transfer is not by ohmic heating.

REFERENCES

1. Giannini Scientific Corporation, "Study of the Factors Affecting the Efficiency in Thermal Acceleration of Propellants," Final Report, Contract AF 49(638)-1161 (August 1965).

2. Avco RAD, "Arcjet Technology Research and Development," Final Report, Contract NAS 3-5900 (December 1965).

3. R. M. Patrick and A. M. Schneiderman, "Performance Characteristics of a Magnetic Annular Arc," Sixth Symposium on Engineering Aspects of Magnetohydrodynamics (1965, p. 70).

4. R. M. Patrick and A. M. Schneiderman, "Study of a Magnetic Annular Plasma Accelerator," Avco Everett Research Laboratory, Summary Report, Contract NAS 3-5748 (January 1966).

5. Electro-Optical Systems, "Hall Current Accelerator," Final Report, Contract NAS 3-5909 (February 1966).

6. Giannini Scientific Corporation, "Design and Development of a Thermo-Ionic Electric Thrustor," Final Report, Contract NAS w-968 (May 1966).

7. A. C. Ducati, G. M. Giannini, and E. Muehlberger, "Experimental Results in High Specific Impulse Thermo-Ionic Acceleration," AIAA J. 2, 1452 (1964).

8. L. Spitzer, Jr., Physics of Fully Ionized Gases, Interscience (1962).

REFERENCES

9. A. C. Ducati, G. M. Giannini and E. Muehlberger, "Recent Progress in High Specific Impulse Thermo-Ionic Acceleration," AIAA Second Aerospace Sciences Meeting, Preprint 65-96 (January 1965).

10. R. G. Jahn and K. E. Clark, "A Large Dielectric Vacuum Facility," Department of Aerospace and Mechanical Sciences, Princeton University, Princeton, New Jersey.

11. R. E. Jones and E. L. Walker, "Status of Large Vacuum Facility Tests of MPD Arc Thrustor," AIAA third Aerospace Sciences Meeting, AIAA Paper No. 66-117 (January 1966).

BLANK PAGE

UNCLASSIFIED

Security Classification

DOCUMENT CONTR ATA - R & D

(Security classification of title, body of abstract and indexing annotation must be entered when the overall report is classified)

1. ORIGINATING ACTIVITY *(Corporate author)*
Giannini Scientific Corporation
Santa Ana Division
Santa Ana, California 92702

2a. REPORT SECURITY CLASSIFICATION
UNCLASSIFIED

2b. GROUP

3. REPORT TITLE

ELECTROTHERMALLY ACCELERATED PLASMA JETS

4. DESCRIPTIVE NOTES *(Type of report and inclusive dates)*
Scientific Final

5. AUTHOR(S) *(First name, middle initial, last name)*

Adriano C. Ducati

6. REPORT DATE	7a. TOTAL NO. OF PAGES	7b. NO. OF REFS
30 September 1966	103	11

8a. CONTRACT OR GRANT NO.
AF49(638)1572

b. PROJECT NO.
9752-01

c.
61445014
681308

9a. ORIGINATOR'S REPORT NUMBER(S)
FR 096-1572

9b. OTHER REPORT NO(S) *(Any other numbers that may be assigned this report)*
AFOSR 66-2726

10. DISTRIBUTION STATEMENT

1. Distribution of this document is unlimited.

11. SUPPLEMENTARY NOTES

12. SPONSORING MILITARY ACTIVITY
AF Office of Scientific Research (SREP)
1400 Wilson Boulevard
Arlington, Virginia 22209

13. ABSTRACT

Experimental and theoretical results are presented on the performance characteristics of the low pressure arc jet operated with hydrogen. Thermal and thrust power efficiency have been measured for up to 20 kilogauss applied magnetic fields and various electrode configurations and specific impulses. The thermal efficiency is insensitive to magnetic field strength and specific impulse in the high range of specific impulse. Thrust efficiency shows a dependence on the magnetic field for operating conditions which produce values of the Hall parameter much larger than unity, but this may be due to the much discussed spurious interactions of the arc with the environment. The efficiencies show a definite and fairly regular increase with increasing arc chamber pressure. Tests have been conducted which demonstrate qualitatively the effect of the applied field on the arc current distribution. A good two-parameter fit of thermal efficiency data is given, and an analytical model for the thermal losses is partially developed. Explicit expressions for the torque on the arc jet flow are obtained for two classes of idealized current distributions. An inequality is derived which places a lower bound on the torque for a given applied magnetic field and electrode configuration.

DD FORM 1 NOV 65 1473

Security Classification

14. KEY WORDS	LINK A		LINK B		LINK C	
	ROLE	WT	ROLE	WT	ROLE	WT
Low Pressure Arc Jet						
Thermal Efficiency						
Thrust Power Efficiency						
Electrode Configurations						
Specific Impulses						
Magnetic Field						
Thrust Efficiency						
Hall Parameter						
Arc Chamber Pressure						
Arc Current						
Thermal Losses						
Torque on the Arc Jet Flow						
Interactions of the Arc with the Environment						